isvr Institute of Sound and Vibration Research

Modelling of Composite Beam Structure

F. Folzan

ISVR Technical Memorandum No 942

September 2004

University of Southampton

SCIENTIFIC PUBLICATIONS BY THE ISVR

Technical Reports are published to promote timely dissemination of research results by ISVR personnel. This medium permits more detailed presentation than is usually acceptable for scientific journals. Responsibility for both the content and any opinions expressed rests entirely with the author(s).

Technical Memoranda are produced to enable the early or preliminary release of information by ISVR personnel where such release is deemed to the appropriate. Information contained in these memoranda may be incomplete, or form part of a continuing programme; this should be borne in mind when using or quoting from these documents.

Contract Reports are produced to record the results of scientific work carried out for sponsors, under contract. The ISVR treats these reports as confidential to sponsors and does not make them available for general circulation. Individual sponsors may, however, authorize subsequent release of the material.

UNIVERSITY OF SOUTHAMPTON

INSTITUTE OF SOUND AND VIBRATION RESEARCH

SIGNAL PROCESSING & CONTROL GROUP

Modelling of Composite Beam Structure

by

M. Folzan

ISVR Technical Memorandum N° 942

September 2004

Authorised for issue by
Prof S J Elliott
Group Chairman

Acknowledgements

Thanks to Prof. S J Elliott who supervised me during the whole project, to Prof P Gardiono for his help and advice about finite element modelling, and to Dr E Rustighi for his aid with the experimental setup.

Abstract

This technical memorandum deals with the modelling of a composite beam structure with a thick layer of rubber attended to an aluminium beam. First, the beam is modelled analytically, then a numerical model is developed, and finally, measurements are carried out on the real beam. Each model has it own limitations, but they do allow different aspects of the behaviour of the beam to be understood, and the numerical model could be further refined and used again for further developments.

Sommaire

Ce memorandum technique traite de la modélisation d'une structure composite de type poutre, composée d'une épaisse couche de caoutchouc liée à une poutre en aluminium. La poutre est tout d'abord modélisée analytiquement, puis un modèle numérique est développé, et finalement, des mesures sont réalisées sur la poutre réelle. Chaque modèle a ses propres limites, cependant ils permettent de comprendre les différents aspects du comportement de la poutre, et le modèle numérique pourra être affiné et réutilisé pour de futurs développements.

Table of contents

Table of illustrations

Table of appendices

List of principal symbols

A	Area of the cross section of the beam
A'	Equivalent area of the aluminium layer
A_1,A_2,A_3,A_4	Amplitudes of the propagating waves in the finite beam
A_{alu}	Area of the aluminium layer cross section
A_{e1},A_{e2}	Amplitudes of the evanescent waves in the finite beam
A_i	Amplitude of the incident wave on the simple support for the infinite beam
A_{n1}	Amplitude of the evanescent wave for $x<0$ near the simple support for the infinite beam
A_{n2}	Amplitude of the evanescent wave for $x>0$ near the simple support for the infinite beam
A_r	Amplitude of the reflected wave by the simple support for the infinite beam
A_{rub}	Area of the rubber layer cross section
A_t	Amplitude of the transmitted wave after the simple support for the infinite beam
b	Width of the beam
c	Celerity of bending waves in the beam
E_{alu}	Young modulus of the aluminium
E_{eq}	Young modulus of the theoretical model
E_{rub}	Young modulus of the rubber
H	Height of the beam
h_{alu}	Height of aluminium
h_{rub}	Height of rubber
I_{alu}	Second moment of inertia of the aluminium layer
I_{eq}	Second moment of inertia of the theoretical model
I_{rub}	Second moment of inertia of the rubber layer
k	Wave number
L	length of the beam
M	Bending moment of the beam
M_{beam}	Total mass of the beam
n	Ratio between the Young moduli of aluminium and rubber
R	Radius of curvature of the beam
R_L	Reflection ratio of the left end of the finite beam
R_n	Reflection ratio of the simple support for the infinite beam
R_R	Reflection ratio of the right end of the finite beam
T_n	Transmission ratio of the simple support for the infinite beam
V_{alu}	Volume of aluminium in the beam
V_{beam}	Total volume of the beam
V_{rub}	Volume of rubber in the beam
$w(x)$	Wave expression in the beam
$w_-(x)$	Wave expression for $x < 0$
$w_+(x)$	Wave expression for $x > 0$
ν_{alu}	Poisson ratio of the aluminium
ν_{rub}	Poisson ratio of the rubber
ρ_{alu}	Density of the aluminium
ρ_{eq}	Density of the theoretical model
ρ_{rub}	Density of the rubber
ρ_{alu}	Stress in the aluminium layer
ρ_{rub}	Stress in the rubber layer

Introduction

Today, with the increasing traffic on the roads, road noise is becoming an important problem. At average driving speeds, road noise appears to be mainly due to tyre vibrations, so if these vibration could be controlled, road noise would significantly be reduced. But before trying to implement active vibration control in tyres, a preliminary study have to be done, in order to investigate the feasibility of control.
The test concept will be to actively control a tyre rolling over a bump, in order to reduce the force transmitted to the tyre by exciting an actuator placed in the tyre belt.

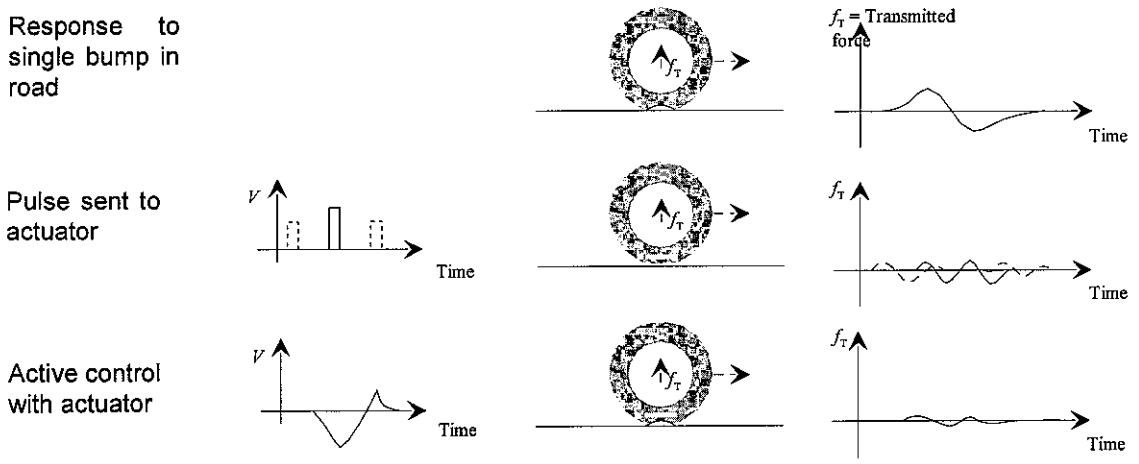

Fig. 1 Experiment concept

However, it is quite difficult to have a simple experience with a controlling system which is rolling. So the problem is reversed: instead of a soft rubber wheel rolling on a hard track, a soft rubber track is rolled over by a hard wheel.

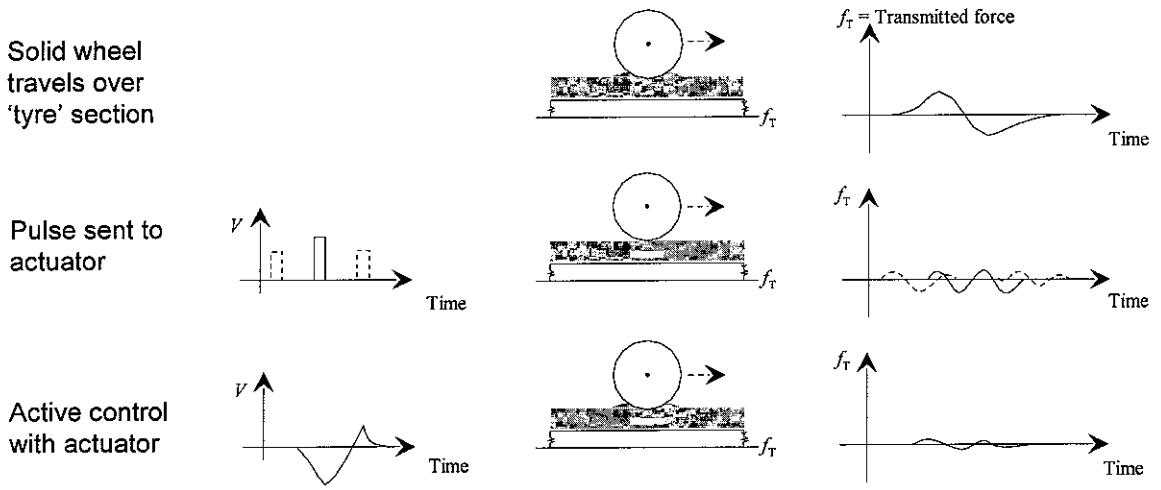

Fig. 2 Experiment procedure

The aim of the study is to characterize the beam structure that will play the role of the track. The first approach to the problem is to take knowledge of the different mechanisms

generating vibrations in a tyre. A general overview of the different theories is given in reference [1].

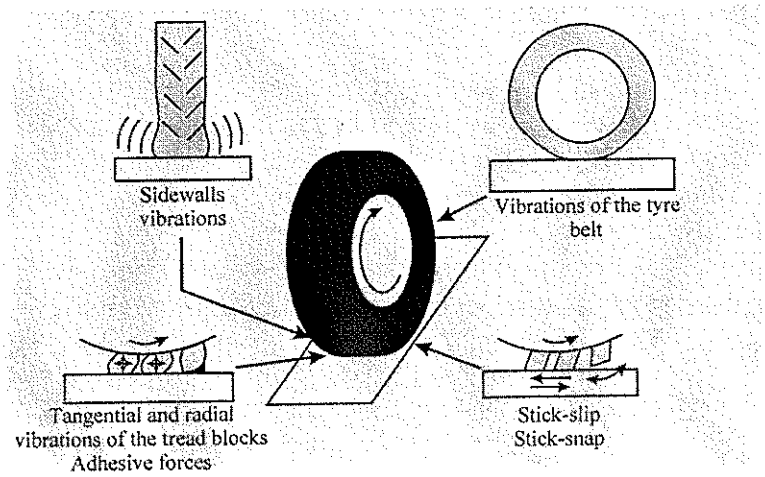

Fig. 3 The different types of tyre vibrations (Reproduced from reference [1])

The most important vibration types are presented in Fig.3. As the tyre is rolling over the road, its sidewalls and its belt are vibrating (they are excited by varying forces). Moreover, at the interface between the tyre and the road, changing contact forces lead to friction mechanisms that produce stick slip as long as the tread is in contact with the road. When the tread are just to leave the road, adhesive forces tend to keep it in contact with the road, and in the same time stick-snap appears. The influence of each of these factors is not easy to determine and they are still investigated, but they are generally agreed and accepted as the noise mechanical sources of a tyre. If active control would be implemented, it could only deal with the sidewalls and belt vibrations.

Different models were developed, particularly the ones by K. Larsson in reference [2] and by J.M. Muggelton *et al* in reference [3]. In reference [2], Larsson utilises a model composed of a flat double-layered plate, supported by an elastic foundation (modelling of the sidewalls and of the pressurised air stiffness) and stretched by an external tension (modelling of the tension due to the internal pressure of the tyre) (see Fig.4). The bottom layer stands for the stiff belt, and the top layer for the tread surface and the behaviour of the tyre is calculated using a wave summation approach.

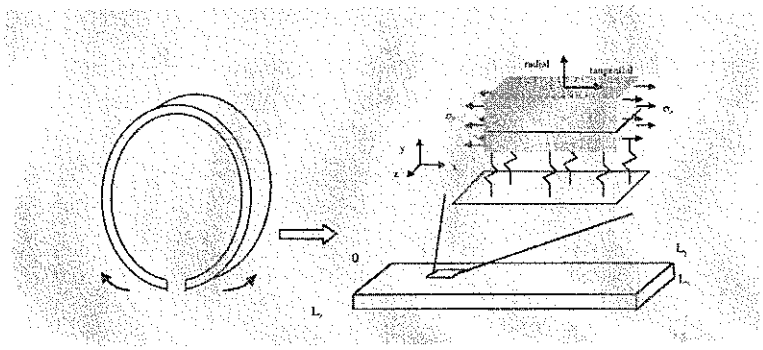

Fig. 4 Model used by Larsson

The model used in reference [3] is very similar: the tyre is seen as an assembly between three orthotropic plates, two plates for the sidewall and one for the tread, with in-plane tension. The edges A and A' are linked by the continuity of slope and displacement, to take in consideration the fact that these two edges are joined in reality (see Fig.5).

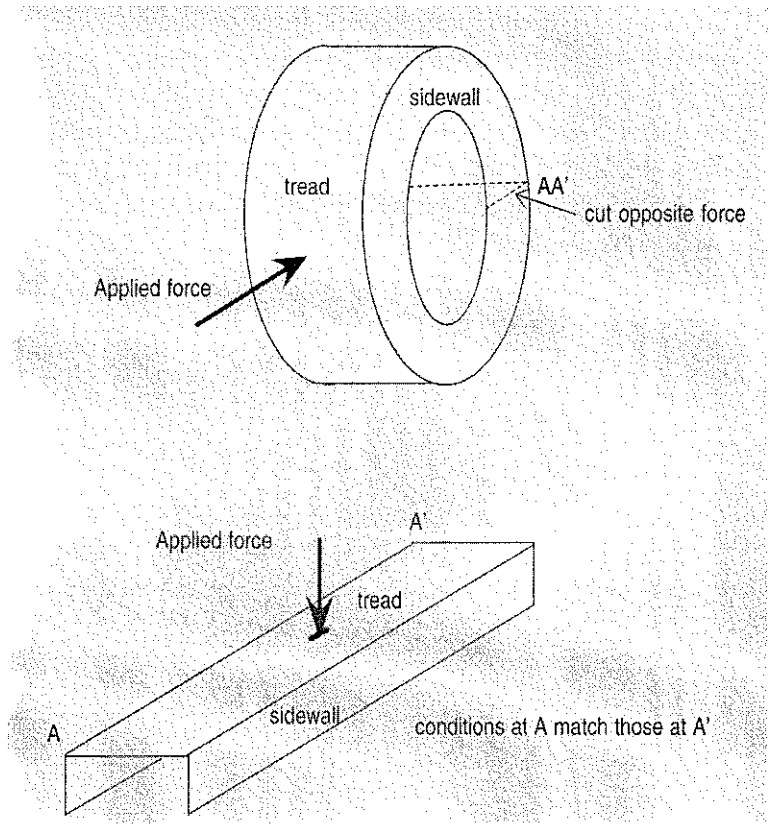

Fig. 5 Model used by Muggleton et al (taken from reference [3])

Another set of boundary conditions is used at the junction between the sidewall and the tread: the are linked by a stiffness, with a continuity of slope.

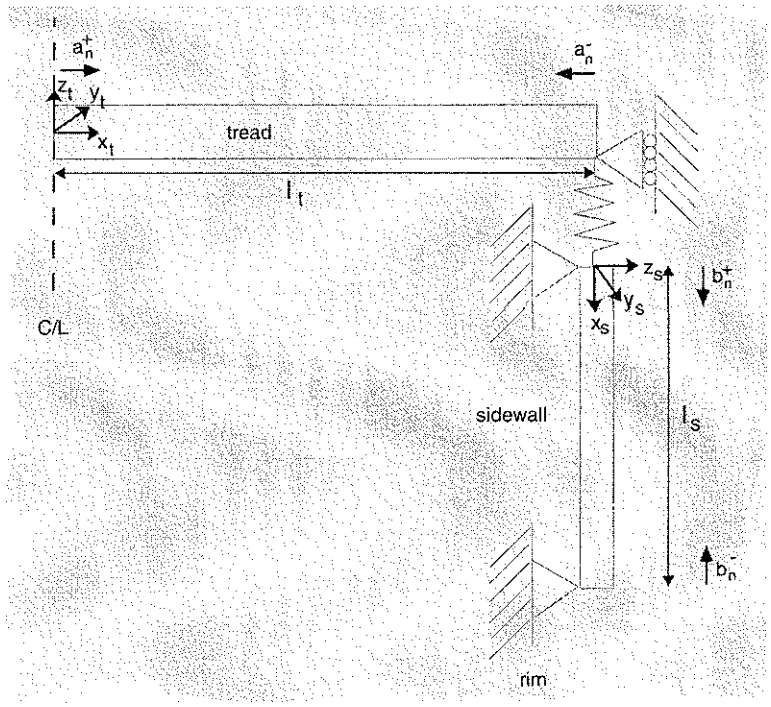

Fig. 6 Junction between the tread and the sidewall

The beam that will be used for the experiment is inspired from these two models; it is composed of two layers, and is supported by three simple supports. Before any measurements, two models are developed: one analytical and one numerical model. The analytical model gives a first idea about the behaviour of the beam and considers only an uniform beam, whereas the numerical one is a composite structure, where the local deformations of the rubber can be seen. Then measurements are made on the real beam.

1 Analytical model

This model is developed in order to predict the mobility of the beam considering one excitation point and one measurement point: the real composite beam is considered to be a uniform beam. A modal approach is used, and the predicted mobility is obtained by a modal superposition method, so the natural frequencies and the modal shapes have to be investigated.

1.1 Properties of the beam

The real track to be used in the experiment is constructed as a composite beam, as shown in Fig. 7, with rubber at the top and an aluminium layer underneath. It is modelled as an equivalent uniform beam: its parameters ρ_{eq}, I_{eq}, and E_{eq} are obtained from the geometrical and structural properties of the real track (see Appendix 1 for the real track data and Appendix 2 for the equivalent uniform beam model data). The beam model is supported by three pinned supports, and only bending in the plane of the figure is considered:

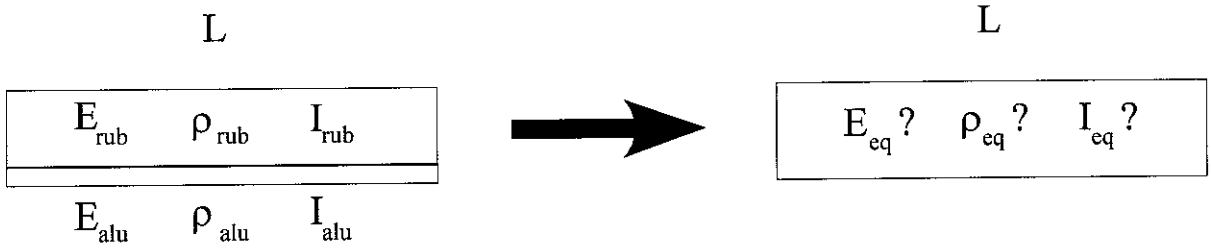

Fig. 7 The composite beam and the equivalent uniform beam model

Several assumptions are made:

a) The resultant of the external forces is a moment that lies in, or is perpendicular to, a plane of symmetry of the cross section

b) The beam is in equilibrium

c) The longitudinal axis of the beam is straight

d) The beam has a constant cross section throughout its length

e) A plane section that is normal to the longitudinal axis of the beam before the beam is bent remains plane after the beam is bent

f) The beam bends without twisting

g) All the materials considered are homogeneous and isotropic

h) The stresses do not exceed the proportional limit of the material

i) The two materials are perfectly bonded together

The easiest parameter to obtain is the equivalent density of the beam:

$$\rho_{eq}=\frac{M_{beam}}{V_{beam}}=\frac{\rho_{alu}\times V_{alu}+\rho_{rub}\times V_{rub}}{V_{alu}+V_{rub}}$$

$$\rho_{eq}=\frac{\rho_{alu}\times h_{alu}+\rho_{rub}\times h_{rub}}{h_{alu}+h_{rub}} \qquad (1)$$

In order to determine I_{eq}, the position of the neutral axis of the real beam needs to be investigated.

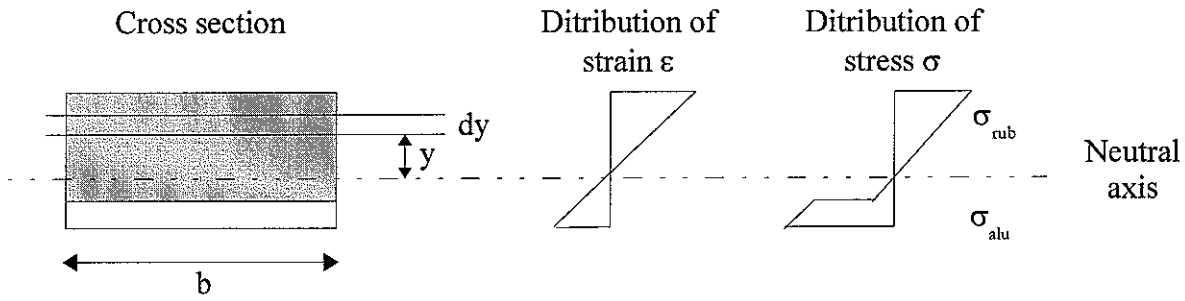

Fig. 8 Stress and strain in the real beam

Using the assumption (i), the strain ε at a level y above the neutral axis is the same in both layers:

$$\varepsilon=\frac{y}{R}$$

So the stresses in the two materials are:

$$\sigma_{rub}=E_{rub}\frac{y}{R} \qquad \sigma_{ralu}=E_{alu}\frac{y}{R}$$

And the total longitudinal force on the layer thickness dy is:

$$(E_{rub}b+E_{alu}b)\frac{y}{R}dy$$

Since the beam is in equilibrium, there is no longitudinal force on the section, and it therfore appears that:

$$\frac{1}{R}\int_{section}(E_{rub}b+E_{alu}b)ydy=0 \qquad (2)$$

If n, the ration between the two Young moduli, is introduced ($n=E_{rub}/E_{alu}$), (2) becomes:

$$\frac{E_{rub}}{R}\int_{section}(1+n)bydy=0$$

$$\frac{E_{rub}}{R}\left(\int_{Arub}bydy+\int_{Aalu}nbydy\right)=0 \qquad (3)$$

If the neutral axis had passed through the centroid of the beam, then $\int_{section} by dy = 0$. But here, the factor n plays a part in the integral: the neutral axis passes through a centroid of a beam where the area of the aluminium cross section is replaced by an equivalent area of rubber n times bigger.

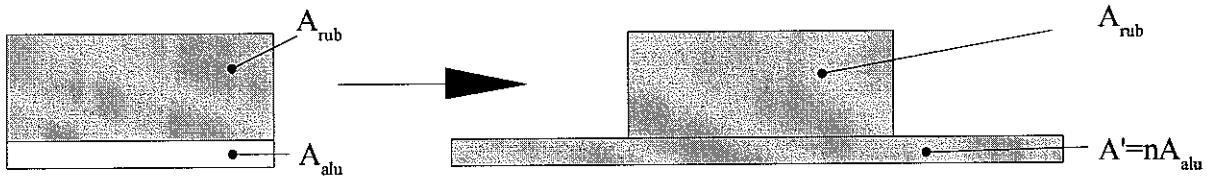

Fig. 9 Replacement of the aluminium layer by an equivalent area of rubber

This method is more detailed in references [1] and [2].
Because of such a Young modulus difference between the two materials, the ratio n is quite high: its value is 2333. So A' is 583 times more important than A_{rub}: it comes out that the centroid of the beam and the centroid of the aluminium layer are the same.
The value of the second moment of inertia of the equivalent beam is (see reference [2]):

$$I_{eq} = I_{rub} + \frac{E_{rub}}{E_{alu}} I_{alu} \approx I_{rub} \tag{4}$$

The last parameter to find is the Young modulus to use for the model.

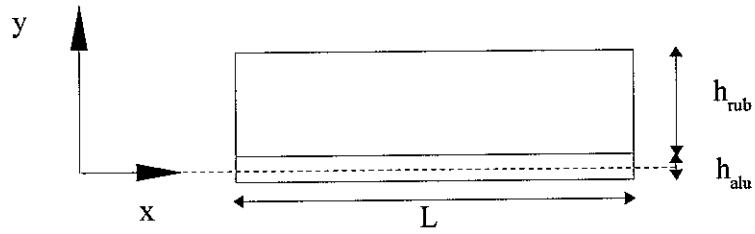

Fig. 10 Side view of the real beam

When bending in the plane of the figure is considered, the total bending moment M is:

$$M = \int_{-h_{alu}/2}^{h_{alu}/2} \frac{E_{alu}}{R} b y^2 dy + \int_{h_{alu}/2}^{h_{rub}} \frac{E_{rub}}{R} b y^2 dy$$

And if E_{eq} is the overall modulus in bending:

$$M = \int_{-h_{alu}/2}^{h_{rub}} \frac{E_{eq}}{R} b y^2 dy \tag{5}$$

Evaluating the integrals, and considering a constant radius of curvature, an expression for E_{eq} can be found:

$$E_{eq} = \frac{2(h_{alu}/2)^3 E_{alu} + (h_{rub}^3 + (h_{alu}/2)^3) E_{rub}}{(h_{alu}/2)^3 + h_{rub}^3} \tag{6}$$

1.2 Bending waves

Once the parameters of the model are defined, the free wave method can be used in order to find the natural frequencies and the mode shapes of the model. The method and some of the calculations are taken from reference [3].
Firstly, the reflection and transmission ratios at a simple support on an infinite beam is considered: only one propagating wave is considered for the moment.

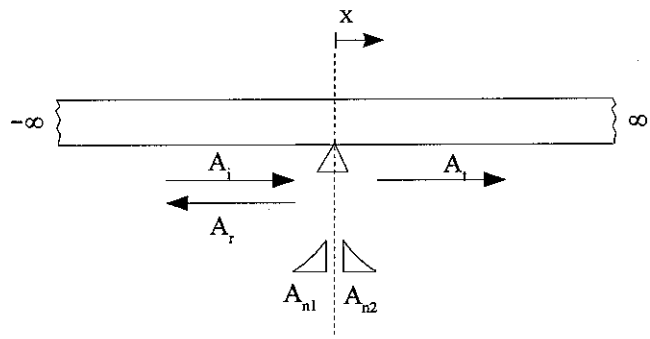

Fig. 11 Waves transmission and reflection in an infinite beam on a simple support

The total wave can be expressed as:

$$\begin{aligned} w(x)=w_-(x)&=A_i e^{-ikx}+A_r e^{ikx}+A_{n1}e^{kx} \quad x\leq 0 \\ w(x)=w_+(x)&=A_t e^{-ikx}+A_{n2}e^{-kx} \quad x>0 \end{aligned} \tag{7}$$

Using the boundary conditions at x=0, some relations can be written between the different amplitudes. If w(0)=0, A_{n1} and A_{n2} can be expressed:

$$A_{n1}=-(A_i+A_r) \tag{8}$$
$$A_{n2}=A_t \tag{9}$$

Using this first boundary conditions, the next conditions give:

$$\begin{aligned} w'_-(0)=w'_+(0) &\Rightarrow -iA_i+iA_r+A_{n1}=-iA_t-A_{n2} \\ &\Rightarrow -(1+i)A_i-(1-i)A_r=(1-i)A_t \end{aligned} \tag{10}$$

$$\begin{aligned} w''_-(0)=w''_+(0) &\Rightarrow -A_i-A_r+A_{n1}=-A_t+A_{n2} \\ &\Rightarrow A_r+A_i=A_t \end{aligned} \tag{11}$$

Combining (11) and (12), an equation can be written between A_r and A_i :

$$\begin{aligned} -(1+i)A_i-(1-i)A_r&=(1-i)A_i+(1-i)A_r \\ \Rightarrow 0&=2(1-i)A_r+2A_i \end{aligned} \tag{12}$$

Now, expressions for R_n and T_n can be found:

$$R_n=\frac{A_r}{A_i}=\frac{-1}{1-i}=\frac{-(1+i)}{2} \tag{13}$$

$$T_n=\frac{A_t}{A_i}=1-\frac{1}{1-i}=\frac{1-i}{2} \tag{14}$$

Once the ratios are found, the finite model of the beam with three simple supports can be considered. The ends of the beam have reflection ratios R_L and R_R, and the ratios at the centre of the beam still are R_n and T_n.

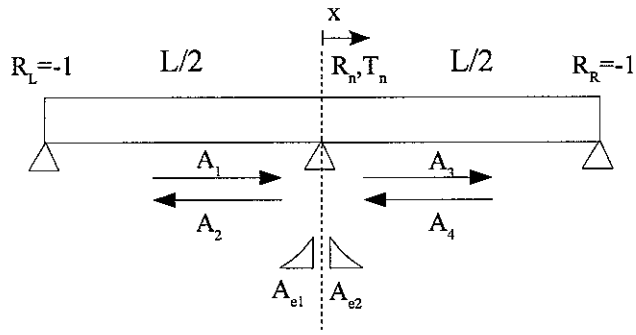

Fig. 12 Waves in the beam model

The evanescent waves in the middle of the beam are caused by the reflection and the transmission of four propagating waves, i.e. A_{e1} is due to the reflection of A_1 and the transmission of A_4 and A_{e2} is due to the reflection of A_4 and the transmission of A_1.

Therefore:

$$A_{e1}=-(1-R_n)A_1-T_nA_4 \quad (15)$$
$$A_{e2}=-T_nA_1-(1-R_n)A_4 \quad (16)$$

The waves equations are now:

-for x<0

$$w_-(x)=A_1e^{-jkx}+A_2e^{jkx}+(-(1-R_n)A_1-T_nA_4)e^{-kx} \quad (17)$$

-for x>0

$$w_+(x)=A_3e^{-jkx}+A_4e^{jkx}+(-T_nA_1-(1-R_n)A_4)e^{-kx} \quad (18)$$

At x=L/2, the A_3 wave has an amplitude $A_3e^{-ikL/2}$ and the A_4 wave, $A_4e^{ikL/2}$. So from reflection ratio, $A_4e^{ikL/2}=R_RA_3e^{-ikL/2}$ i.e. $A_4=-A_3e^{-2ikL/2}=\frac{-A_3}{\gamma}$ with $\gamma=e^{2ikL/2}$. Similarly, at x=-L/2, $A_1=-A_2e^{-2ikL/2}=\frac{-A_2}{\gamma}$.

At the centre (x=0)of the beam:

$$A_2=A_1R_n+A_4T_n \quad (19)$$
$$A_3=A_4R_n+A_1T_n \quad (20)$$

When A_2 and A_3 are substituted in (20) and (21)

$$-\gamma A_1=A_1R_n+A_4T_n \Rightarrow -A_1(\gamma+R_n)=A_4T_n$$
$$-\gamma A_4=A_4R_n+A_1T_n \Rightarrow -A_4(\gamma+R_n)=A_1T_n$$

$$\Rightarrow \frac{-A_1}{A_4}=\frac{T_n}{\gamma+R_n}=\frac{\gamma+R_n}{T_n} \quad (21)$$

$$\Rightarrow T_n^2=(\gamma+R_n)^2 \quad (22)$$

If (14) and (15) are subsituted in (22) and (23), a solution for k can be found:

$$\left(\frac{1-i}{2}\right)^2=\left[\gamma\frac{(1+i)}{2}\right]^2 \tag{23}$$

The solutions for γ are:

$$\gamma=e^{2ikL/2}=\frac{1+i}{2}\pm\frac{\sqrt{(1+i)^2-4i}}{2}=\frac{1+i}{2}\pm\frac{1-i}{2}=1\ or\ i \tag{24}$$

Hence k can have several different values:

-for $\gamma=1$

$$k=\frac{n2\pi}{L} \tag{25}$$

-for $\gamma=i$

$$k=\frac{(n+1/4)2\pi}{L} \tag{26}$$

The value of k in (25) gives the mode shapes displayed in appendix 4, 6 and 8: they are similar to the ones obtain with a beam on two simple supports. On the other hand, if the value in (26) is considered, the mode shapes in appendices 5 and 7 are obtained: the simple support in the middle of the beam acts as a clamped end for both sides.
When γ is introduced in equation (18) and (19), they becomes:

$$w_-(x)=A_1[-\gamma e^{-ikx}+e^{ikx}+(\gamma-1)e^{kx}] \tag{27}$$
$$w_+(x)=A_4[-\gamma e^{-ikx}+e^{ikx}+(\gamma-1)e^{-kx}] \tag{28}$$

The modal shapes are the imaginary parts of the waves equations.
Once k is obtained, the natural frequencies can be derived from k considering the celerity of bending waves $c=\omega^{1/2}\left(\frac{E_{eq}I_{eq}}{\rho_{eq}A}\right)^{1/4}$:

$$kc=\omega=2\pi f$$

$$\Rightarrow f=\frac{k^2}{2\pi}\left(\frac{E_{model}I_{model}}{\rho_{model}A}\right)^{1/2} \tag{29}$$

As soon as the natural frequencies and the mode shapes are known, a modal superposition method is used to determine the mobility of the beam according to excitation and response locations:

$$M(\omega)=\omega\sum_{i=1}^{N}\frac{(\Phi_i)_r(\Phi_i)_f}{\omega_i^2-\omega+2\xi_i\omega_i\omega} \tag{30}$$

Where $(\Phi_i)_r$ is the value of the mode shape at the excitation point and $(\Phi_i)_r$ the value of the mode shape at the response point, and ω_i and ξ_i the natural pulsation and the modal damping of the mode. It is this expression for the mobility which is used when the mobility is referred as the one calculated with the analytical model, with the modal damping is evaluated at 0.07, as the average modal damping measured from 0 Hz to 2 kHz on the real beam.

2 Finite element model

A finite element (FE) model the beam was developed in order to provide an alternative description of the behaviour of the beam. In this case three dimensional motion is considered, and local deformations appears and this model also takes into account the fact that the beam is composite. The mobility is also computed for the FE model and compared with the mobility obtained with the analytical one.

2.1 Description of the model

The model has the same properties as the real beam: it is composed of two materials, and is on three simple supports.
The dimensions of the model are the same as the real beam ones (See Appendix 1). Each material layer is modelled by a different type of element.

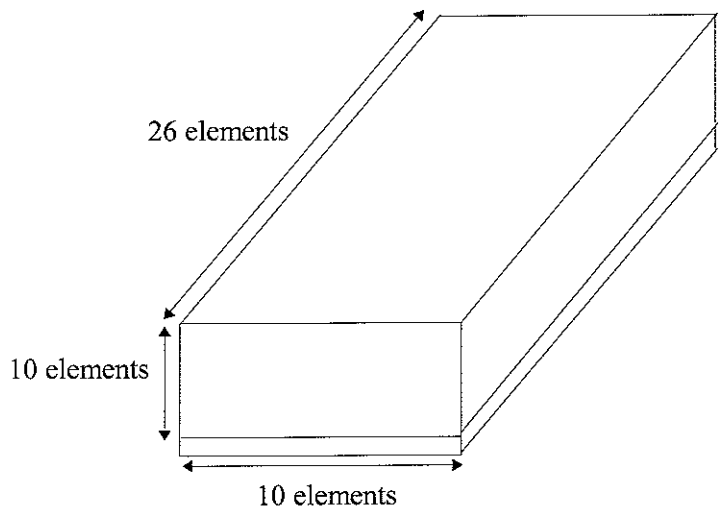

Fig. 13 Mesh definition of the beam

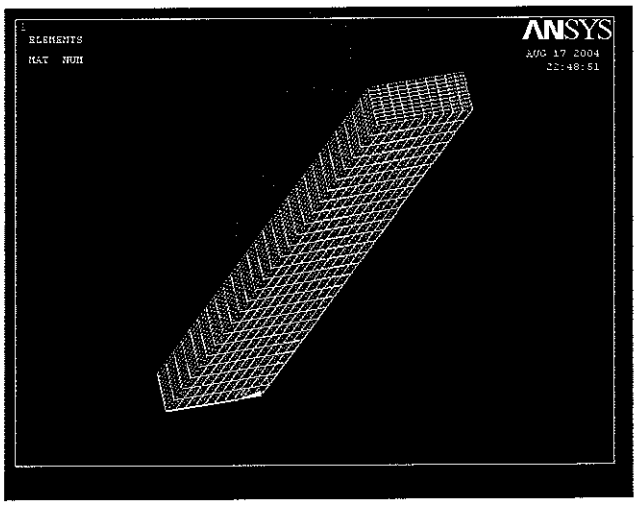

Fig. 14 View of the mesh in the simulation software

For the aluminium layer, a shell element is employed, described in Fig. 15.

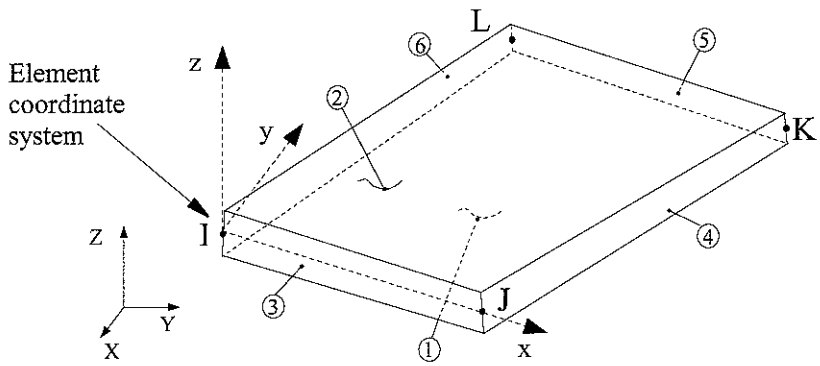

Fig. 15 Geometry of the shell element used for the aluminium layer

This element is composed of four nodes (I, J, K, L) that have six degrees of freedom each. The thickness of the element also have to be defined: it is set to 3 mm. The material properties of the element are E_{alu}, ρ_{alu} and ν_{alu} . This type of element is called SHELL63 in reference [4].
The rubber layer is modelled in another way; a three dimensional solid element is used (see Fig. 16).

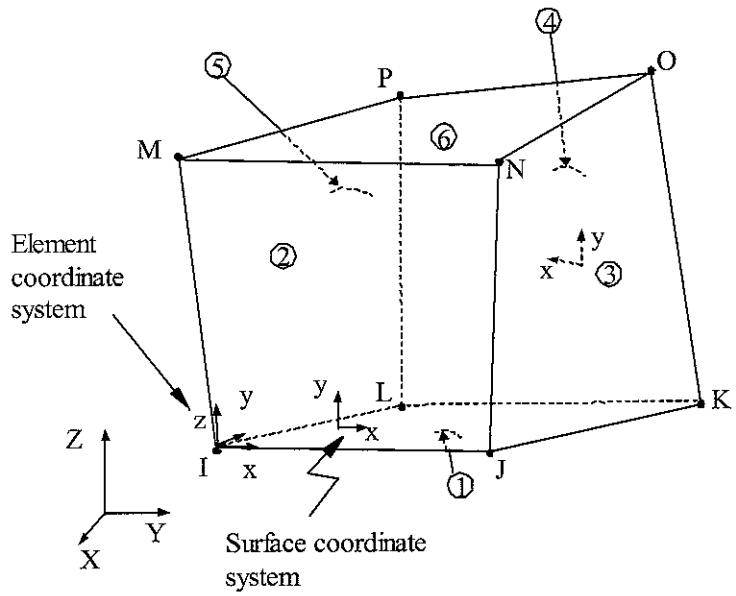

Fig. 16 Geometry of the solid element used for the rubber layer

In order to define the mesh, a parallelepiped is created using the FE software: one face of the volume is meshed with shell elements, and the inner volume is filled with solid element. The junction between the two elements is made by the software, assuming continuity of displacement and slope.

2.2 Results obtained

First, a modal analysis was made, in order to compare the computed bending modes with the ones obtained with the analytical model. The results are displayed in appendix 9 for the

natural frequencies and in appendix 10 to 16 for the modal shapes. The frequencies obtained with the two models are quite close, even if two additional modes appears before 2 kHz with the numerical model. The general modal shapes are similar in the two models, and the deformation of the rubber layer appears with the finite elements model.

Another way to compare the two models is to obtain the mobility between two points of the beam. The result is displayed in the following figure, with an excitation point 9.2 cm and a response measured at 20.7 cm from the edge of the beam. The two points are initially considered in the aluminium layer of the FE model, so the rubber deformation is not taken into consideration.

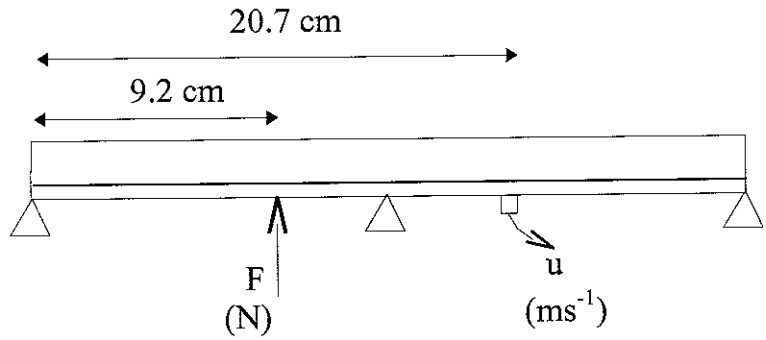

Fig. 17 Exemple of positions of the excitation force and of the measurement point

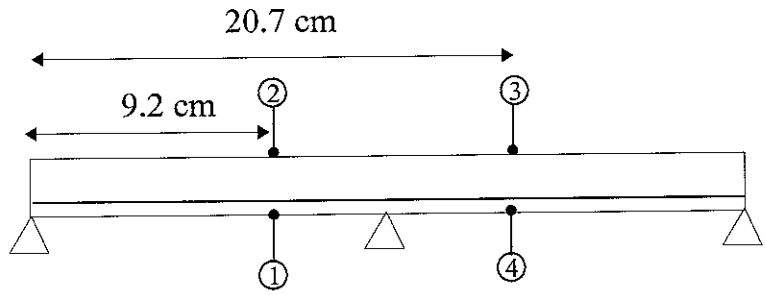

Fig. 18 Position of the different points used

The force is then considered to act at either point 1 (in the aluminium layer) or 2 (in the rubber layer), and the response is measured at point 3 (in the aluminium layer) or 4 (in the rubber layer). Only the most important results will be displayedbelow, but all the mobilities are presented in appendicces 17 to 25.

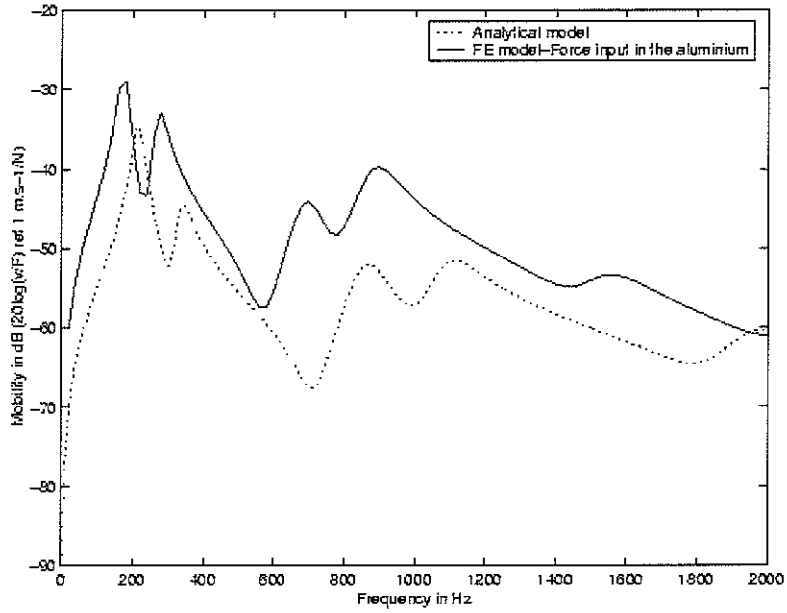

Fig. 19 Input mobility at point 1 (in the aluminium layer)

Even though the FE model mobility is above the one obtained with the analytical model, the two curves have a very similar shape: each mode can be clearly identified.. The modal damping is considered constant for each mode, at 0.07 – This value has been determined from an average of the damping ratios of the real beam, after measurements made in part 3.

If the force acts on the rubber, at point 2, the two mobilities are very different: however the analytical model does not take into account the local displacement of the rubber layer, and significantly under-predicts the mobility above 500Hz.

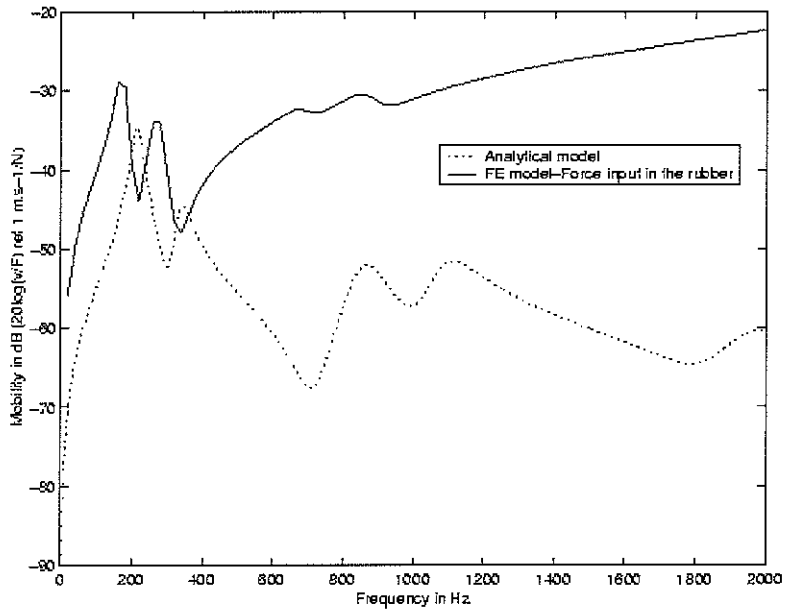

Fig. 20 Input mobility at point 2 (in the rubber layer)

The local deformation can be seen in the following figures: in these cases, the displacements at the bottom of the aluminium layer are blocked. It is as if the beam was clamped to its support. The mesh is also refined, there is two times more elements in the length of the beam. The beam is stressed by two sets of forces to give the result displayed in Fig.21: initially four forces are distributed over the nodes of a 2x2 nodes square. The second configuration is a set of nine forces stressing a 3x3 nodes square (the total force is always equal to one in the both cases).

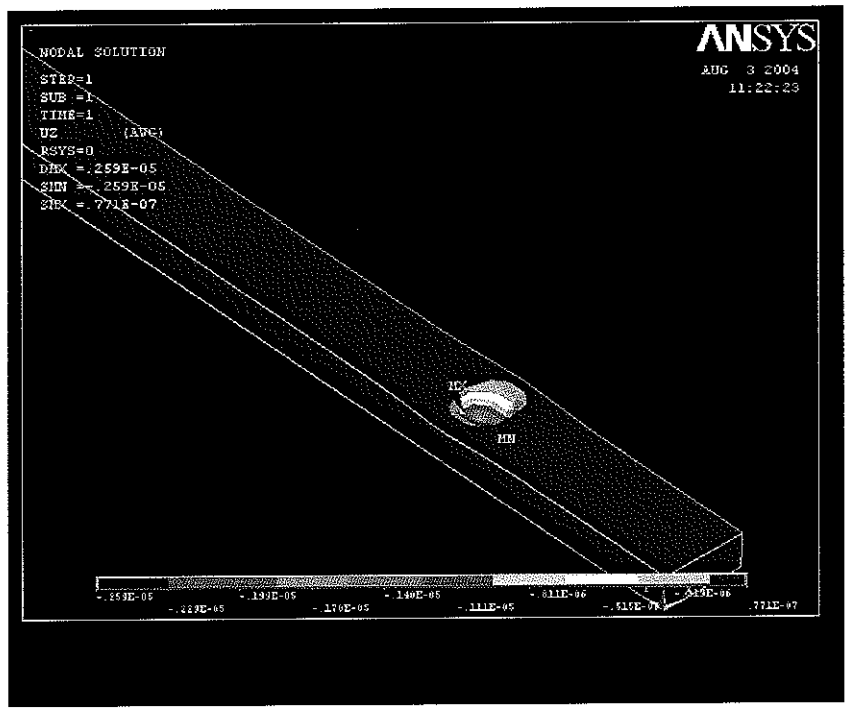

Fig. 21 Displacement of the rubber layer under a static force on a 2x2 node square

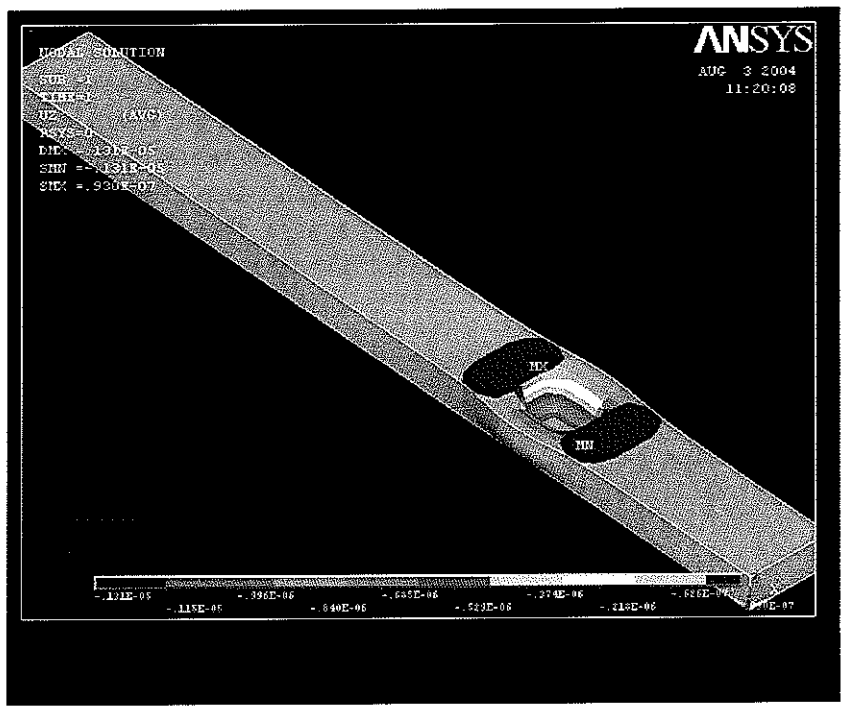

Fig. 22 Displacement of the rubber layer under a static force on a 3x3 nodes square

Note that even if the displacements seem more important in the second case, the colour scale and the displayed displacement are not the same in the two cases since they are set by the simulation software. When subjected to a force, the rubber expands in the longitudinal sides of the beam and a bit in the surface of the layer.

The influence of the rubber in the bending plane of the beam is similar to the one of a spring stressed by a force. When a force is applied in the bending plane, it can be seen as a force acting on two springs in series, which stiffnesses are due to the rubber and the bending movement.

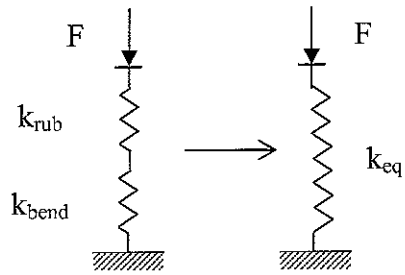

Fig. 23 Action of the rubber

According to this model, $k_{eq} = \frac{k_{bend} \times k_{rub}}{k_{bend} + k_{rub}}$.

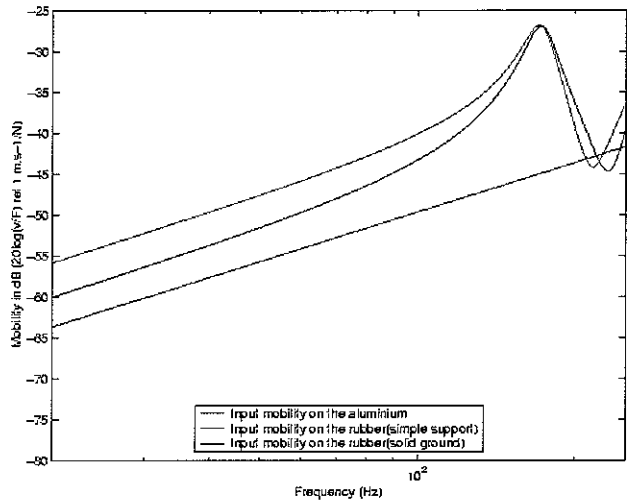

Fig. 24 Behaviour of the beam in low frequencies for different configurations

In the figure above, the green line is the input mobility obtained at point 2, i.e. in the rubber, with the beam on a simple support, so the stiffness obtained using this curved should be k_{eq}. The red line is the same input mobility, but the beam is clamped to the ground, and only k_{rub} should have an influence. The blue line is the input mobility with a beam on its three simple supports, but with the force input at point 1, in the aluminium layer, Therefore, k_{bend} is the only stiffness that should appear. The stiffness is directly related to the height of the curve, when $F=kx=\frac{k}{\omega}v$, and if $Y=\frac{v}{F}$, so $\log(k)=\log(\omega)-\log(Y)$.

Here are the different values obtained for the stiffnesses:

k_{rub} (obtained from the mobility)	$1.81\text{x}10^5$ N/m
k_{bend} (obtained from the mobility)	$1.21\text{x}10^5$ N/m
k_{eqmob} (obtained from the mobility)	$7.61\text{x}10^4$ N/m
k_{eqcal} (calculated from the previous model the mobility using k_{rub} and k_{bend})	$7.27\text{x}10^4$ N/m

3 Behaviour of the real beam

After having studied the general behaviour of the beam in section 1, and having modelled the beam in section 2, the finite element mobilities are compared to measurements made on the real beam

3.1 Experimental setup

The track is supported by three fixed rods, at its two ends and the middle: see Fig.25. The distance between the two ending rods is 300 mm, and a shaker excites the beam in its quarter length. The two force transducers drawn between the rods and the beam in the figure were used for other experiments which are not relevant here.

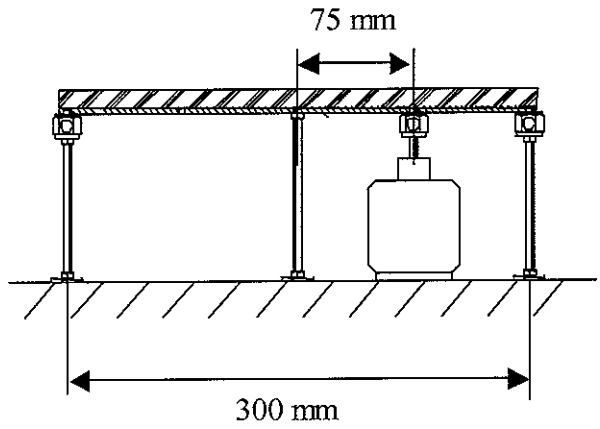

Fig. 25 Setup of the track

A white noise signal is send to the shaker: the input force is measured by the force transducer PCB type 8200, serial 1288285, fixed between the shaker and the beam, and the response is obtained with the accelerometer PCB type 4375, serial 0987252, at several positions, explained in Fig.26.

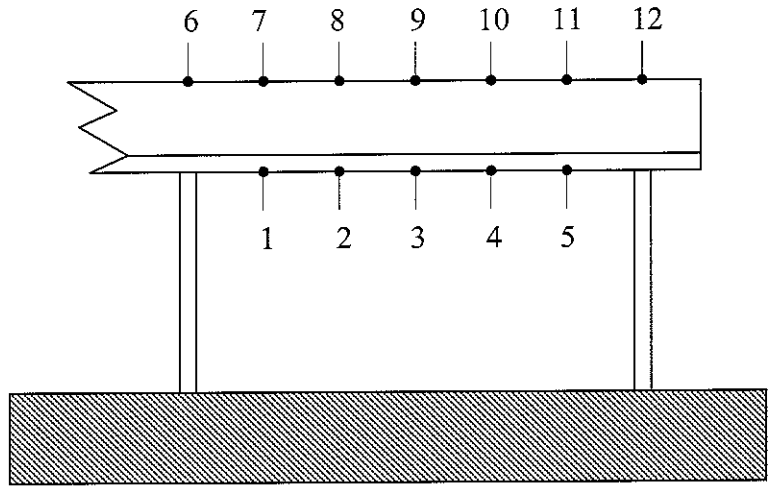

Fig. 26 Points measured on the beam

Two measurement sets are made: one with point 3 as excitation point, and another one where this role is played by point 9. In this last configuration, the force transducer is not fixed to the rubber layer, but the shaker is set in order to slightly prestress the rubber, and contact is maintain in this way. The screw of the force transducer is in direct contact with the rubber surface and allows to inject a "point" force.

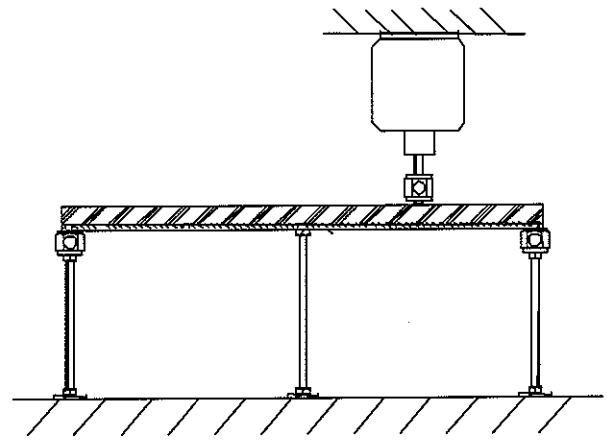

Fig. 27 Schematic representation of the setup when the force is input in the rubber

A dual channel analyzer is used, and recorded response spectra contain 800 lines from 0 Hz to 2kHz.

3.2 Results

Only the representative results are displayed in this section. However, all the spectra are in appendices 27 to 50.

3.2.1 Force input in aluminium layer

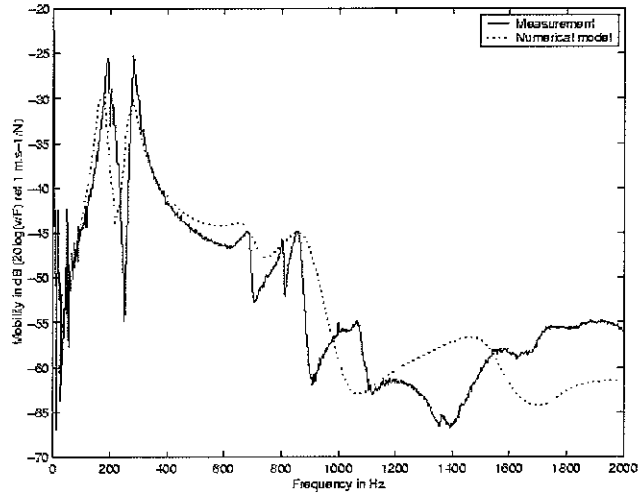

Fig. 28 "Input" mobility at point 3 (input and measurement point in the aluminium)

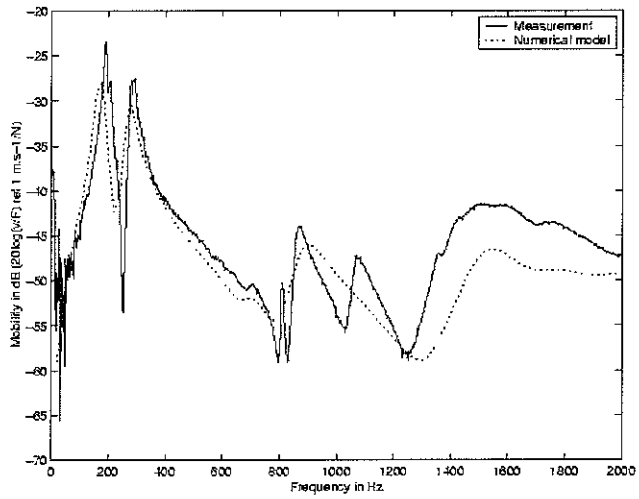

Fig. 29 Mobility between point 3 (input force in the aluminium) and point 3 (measured velocity in the rubber)

The mobility is close to predicted one, especially for the two first peaks. In general, the two curves are close, except at points in rubber near the support. Yet, in the model, the beam is supported by a perfect simple support, on a single line of nodes, whereas in reality, the beam is fixed by the screwed rod: this could explain the differences. The "input" mobility cannot be exactly measured due to the physical dimension of the force transducer, so the accelerometer is placed as close as possible to the input point.

3.2.2 Force input in rubber layer

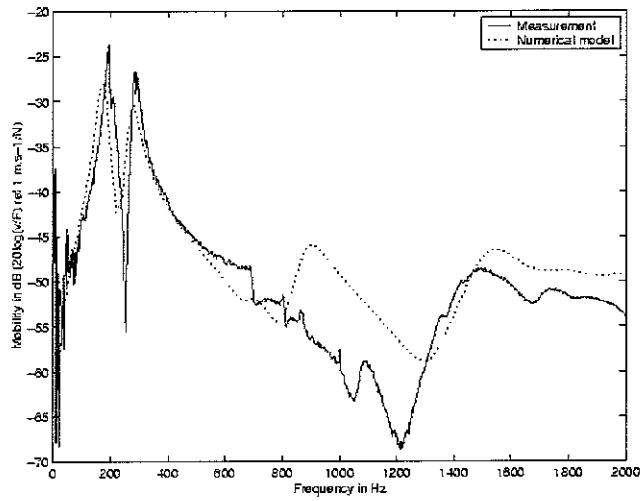

Fig. 30 Mobility between point 9 (input force in the rubber) and point 3 (measured velocity in the aluminium)

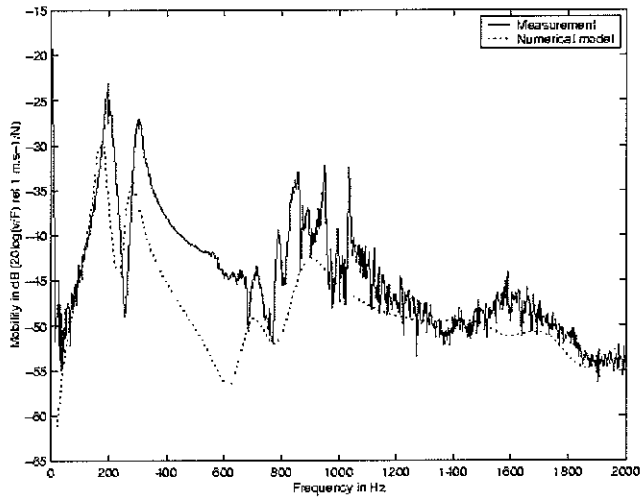

Fig. 31 Mobility between point 9 (input force in the rubber) and point 8 (measured velocity in the rubber)

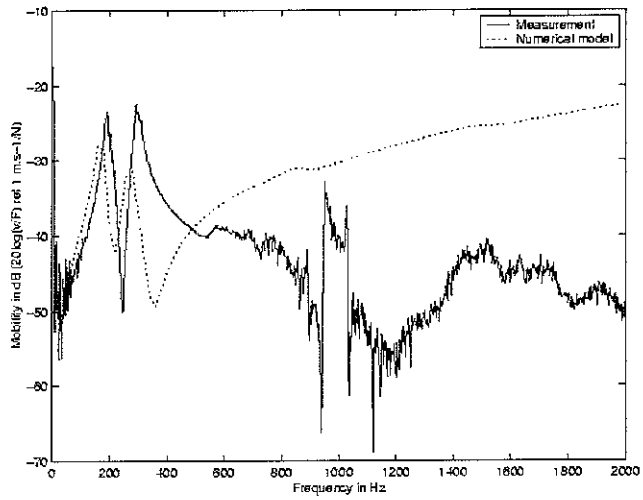

Fig. 32 "Input" mobility at point 9 (input and measurement points in the rubber)

When the force is input in the rubber, despite the fact that the shaker and the layer are not fixed together, the two curves are similar when the measurement point is in the aluminium layer. When response in the rubber layer is considered, the transfer becomes noisy above 700 Hz, but the behaviour seems to be the same.
The measured input mobility is very different: the measurement point was not really the input point, but as close as possible considering accelerometer and force transducer sizes. The FE model takes into account the local deformation when the mobility is computed between the same two points, with the aluminium layer fixed to the ground.

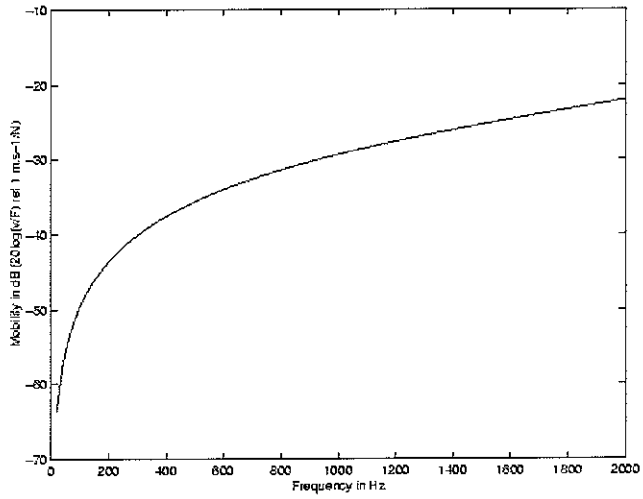

Fig. 33 Input mobility computed at point 9 (input and measurement points in the rubber)

4 Conclusion

The analytical model allowed the overall behaviour of the composite structure to be understood. This model is validated by the FE simulation, because even if it is only an approximate modle of the composite beam, the overall shape of the mobility fits quite well with the ones obtained with the FE model.
As for the FE model, the results obtained are really close to the ones measured on the real beam when it is excited on either the rubber or the aluminium. By using this model in the future, the predicted behaviour of the strucure when excited by piezoelectric actuators and rolled over by a steel wheel may be a good representation of what is happening in the real beam. It is also useful to have a such model, since the local behaviour of the beam can be investigated.
However, the validity of the model regarding local deformations has not been studied in detail. As rubber is a very elastic material, whose properties are sometimes hard to determine, specially its damping ratio, further developments could be done in this area. The results obtained could be compared to the results on real tyres presented in references [1] and [3].

References

[1] W. Kropp, K. Larsson, F. Wullens, P. Andersson, F.-X. Bécot, "*The Generation of Tyre/Road Noise- Mechanisms and models*" , Tenth International Congress on Sound and Vibration, Stockholm; Sweden, 2003

[2] K. Larsson, "*Modelling of Dynamic Contact – Exemplified on the Tyre/Road Interaction*" , PhD Thesis, Department of Applied Acoustics, Chalmers University of Technology, Göteborg, Sweden, 2002

[3] J.M Muggleton, B.R Mace, M.J Brennan, *"Vibrational response of a pneumatic tyre using an orthotropic two-plate model"*, Journal of Sound and Vibration, 264 929-950, 2003

[1] J.R. Tyne, *Simple bending*, Chatto & Windus Ltd, 1974

[2] Glenn Murphy, *Advanced Mechanics of Materials*, McGraw-Hill Book Company Inc., first edition, 1946

[3] D.J. Thompson, *Problem sheet 2 in High Frequency Structural Vibration module*, MSc Sound and Vibrations Studies at the ISVR

[4] ANSYS Incorporated, *ANSYS Release 8.1 Documentation preview*

Appendices

L x b x h	300 x 30 x 15 mm
E_{alu}	70 GPa
ρ_{alu}	2700 kg/m^3
ν_{alu}	0,35
h_{alu}	3 mm
A_{alu}	90 mm^2
E_{rub}	30 MPa
ρ_{rub}	1500 kg/m^3
ν_{rub}	0,5
h_{rub}	12 mm
A_{rub}	360 mm^2

Appendix 1 Properties of the real beam

A	4.5 e -4 m^2
E_{eq}	303 MPa
ρ_{eq}	1740 kg/m^3
I_{eq}	2.457e-8 m^4

Appendix 2 Properties of the analytical model

Number of the mode	Wave number (m^{-1})	Natural frequency of the mode (Hz)
1	21	215
2	26	336
3	42	861
4	47	1090
5	63	1937

Appendix 3 Natural frequencies obtained woth the analytical model

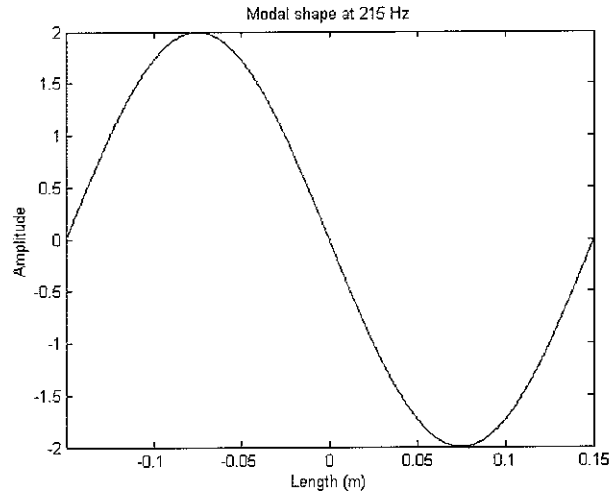

Appendix 4 Mode shape obtained at 215 Hz

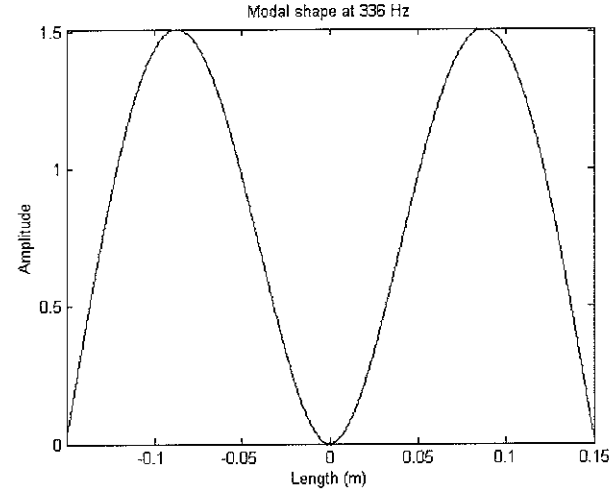

Appendix 5 Mode shape obtained at 336 Hz

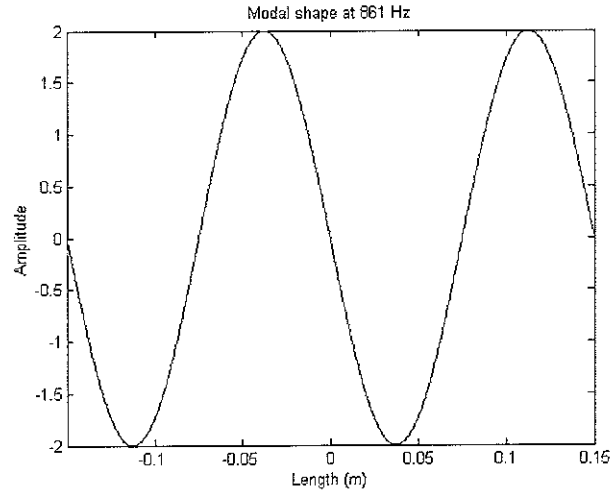

Appendix 6 Mode shape obtained at 861 Hz

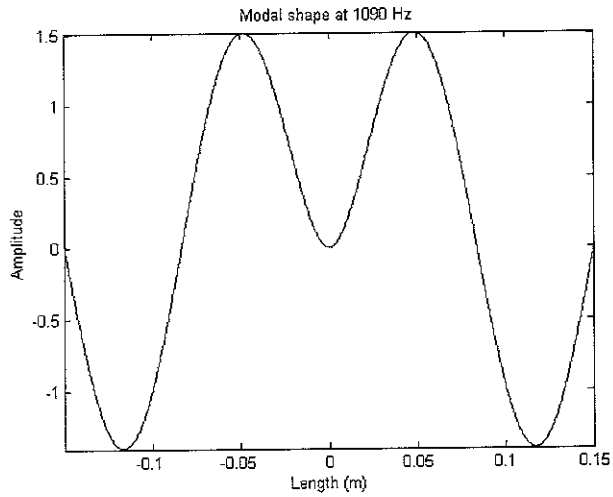

Appendix 7 Mode shape obtained at 1090 Hz

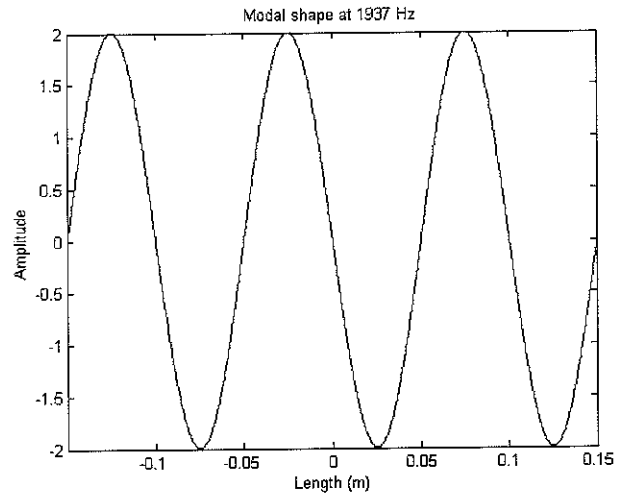

Appendix 8 Mode shape obtained at 1937 Hz

Number of the mode	Natural frequency(Hz) in the analytical model until 2kHz	Natural frequency (Hz) in the numerical model until 2kHz
1	215	172
2	336	271
3	861	690
4	1090	877
5	1937	1516
6	n/a	1635
7	n/a	1745

Appendix 9 Natural frequencies obtained with the two models

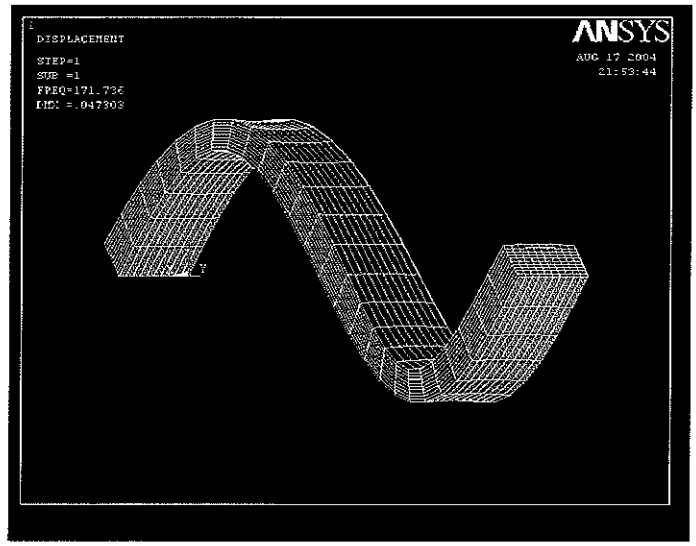

Appendix 10 Mode shape - First mode of the numerical model (172 Hz)

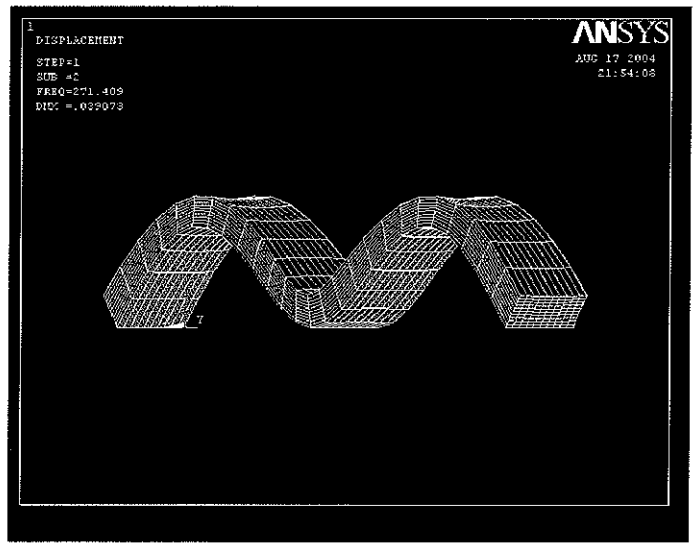

Appendix 11 Mode shape - Second mode of the numerical model (291 Hz)

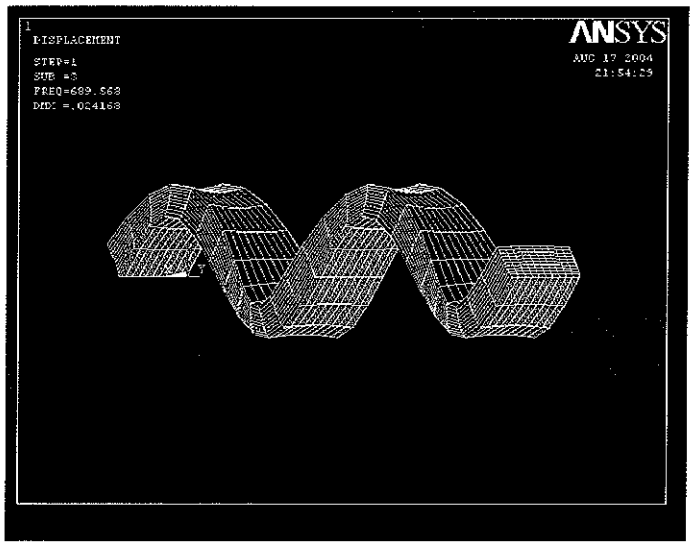

Appendix 12 Mode shape - Third mode of the numerical model (690 Hz)

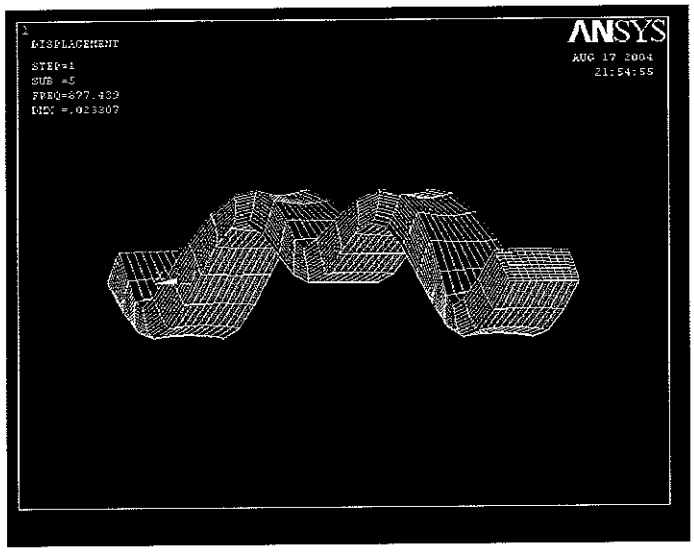

Appendix 13 Mode shape - Fourth mode of the numerical model (877 Hz)

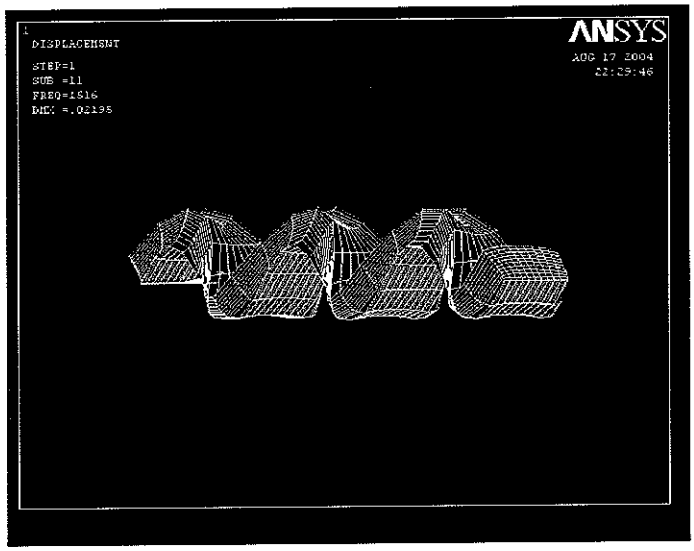

Appendix 14 Mode shape - Fith mode of the numerical model (1516 Hz)

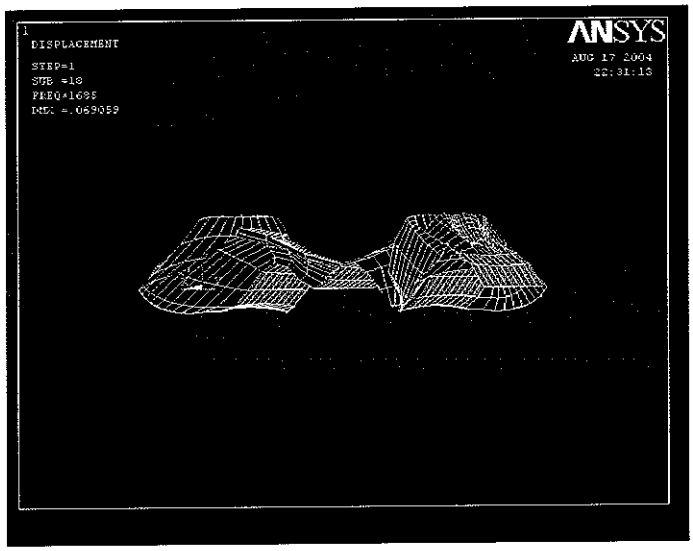

Appendix 15 Mode shape - Sixth mode of the numerical model (1685 Hz)

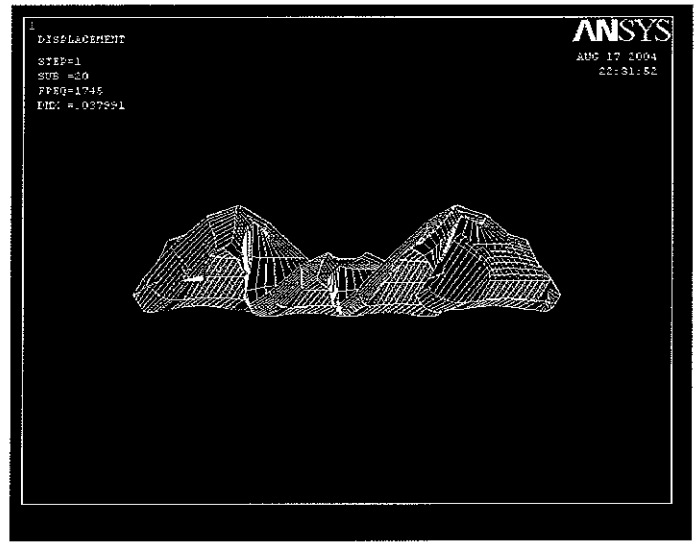

Appendix 16 Mode shape – Seventh mode of the numerical model (1745 Hz)

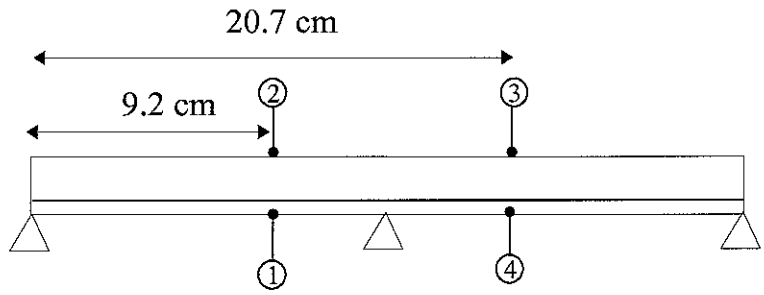

Appendix 17 Position of the different points on the beam or appendices 17 to 25

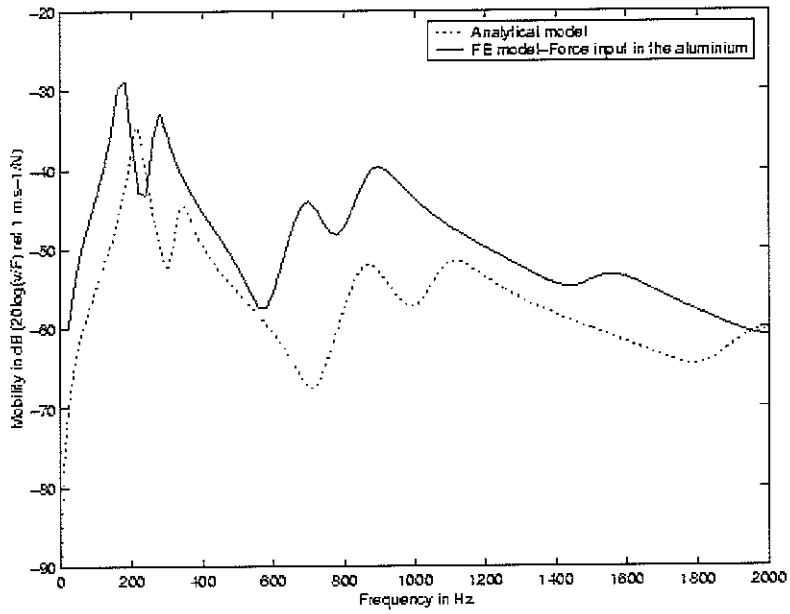

Appendix 18 Input mobility at point 1 (point situated in the aluminium)

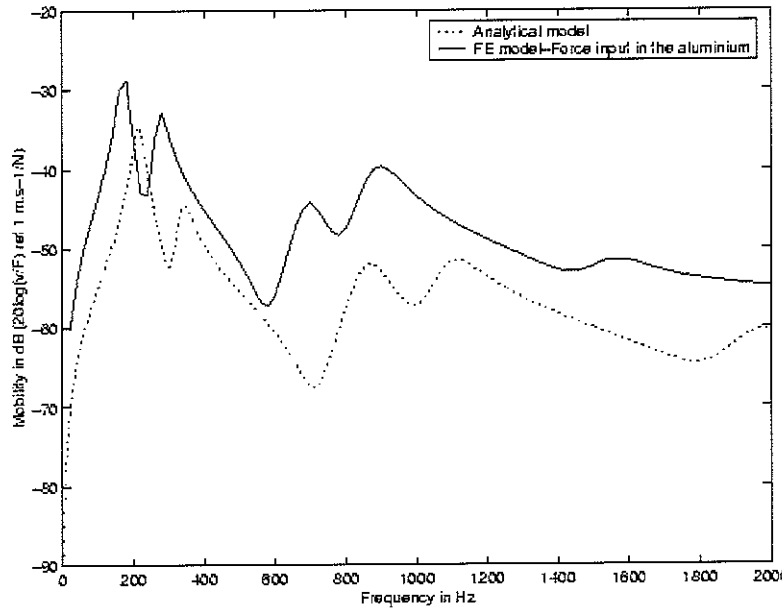

Appendix 19 Transfer mobility between point 1 (input force in the aluminium) and point 2 (measured velocity in the rubber)

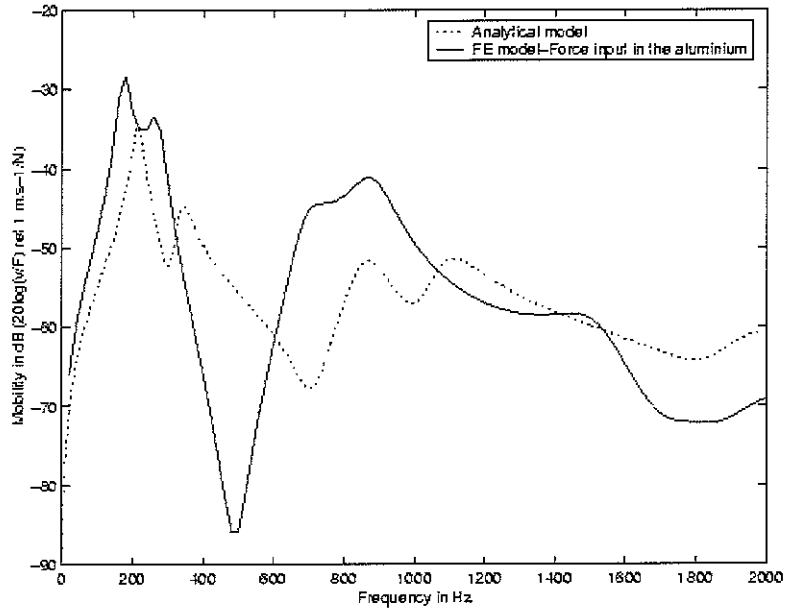

Appendix 20 Transfer mobility between point 1 (input force in the aluminium) and point 3 (measured velocity in the aluminium)

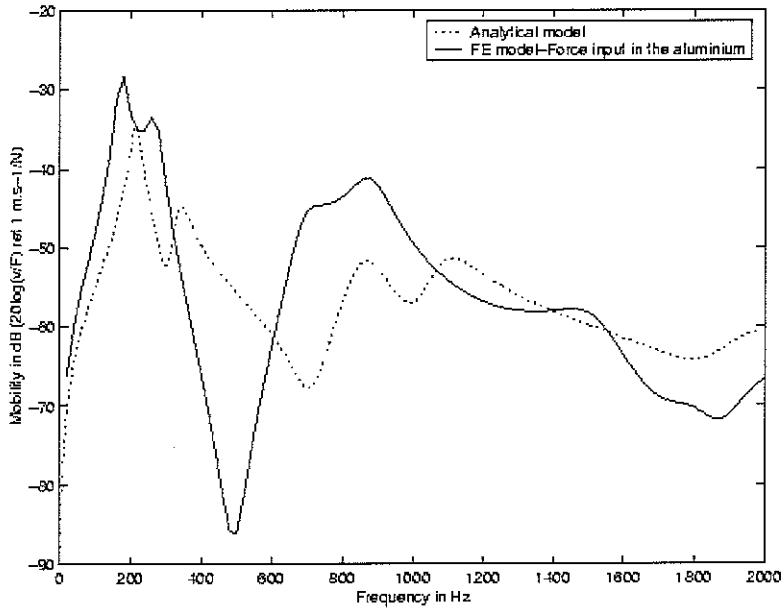

Appendix 21 Transfer mobility between point 1 (input force in the aluminium) and point 4 (measured velocity in the rubber)

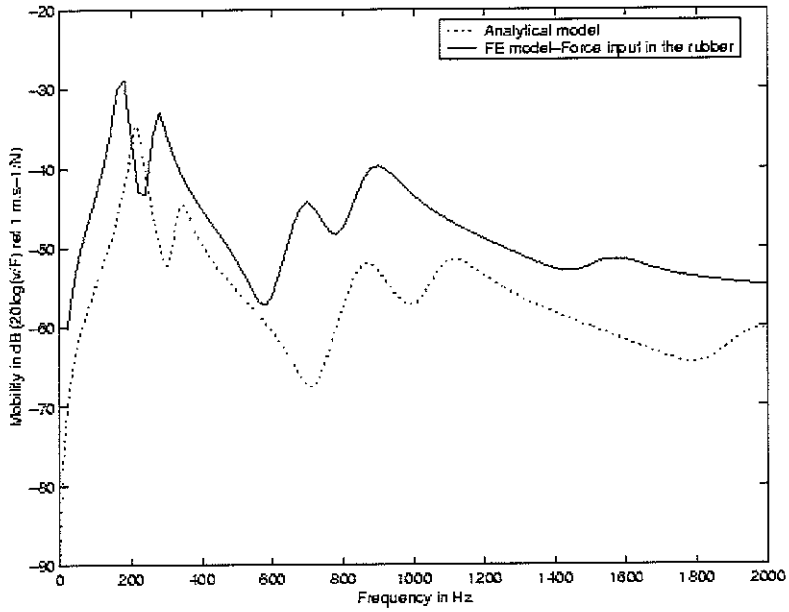

Appendix 22 Transfer mobility between point 2 (input force in the rubber) and point 1 (measured velocity in the aluminium)

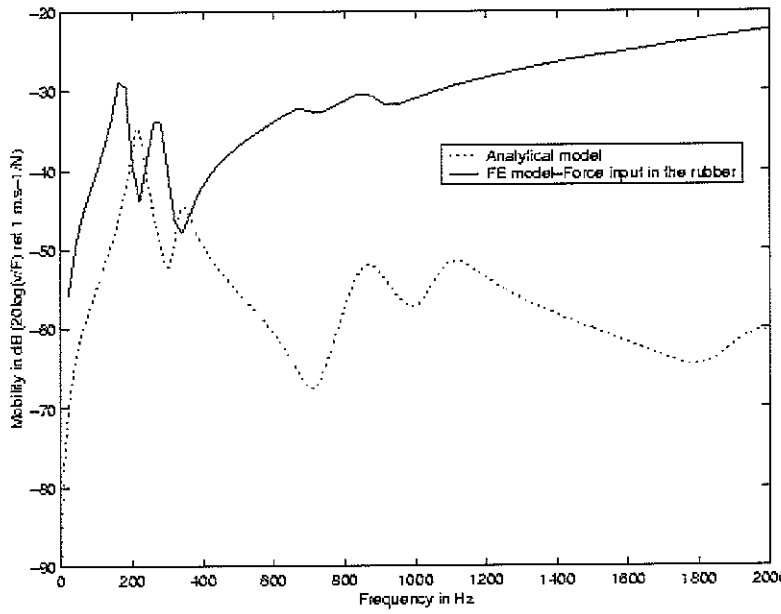

Appendix 23 Input mobility at point 2 (point in the rubber)

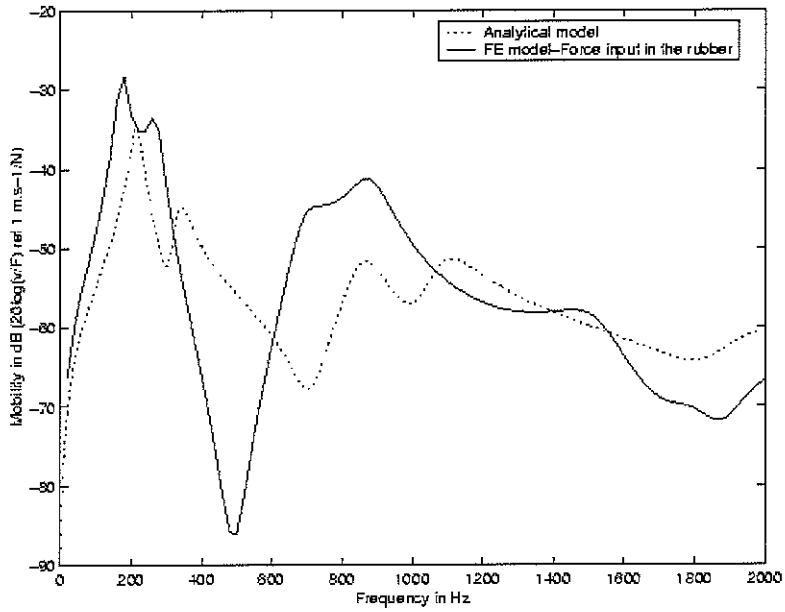

Appendix 24 Transfer mobility between point 2 (input force in the rubber) and point 3 (measured velocity in the aluminium)

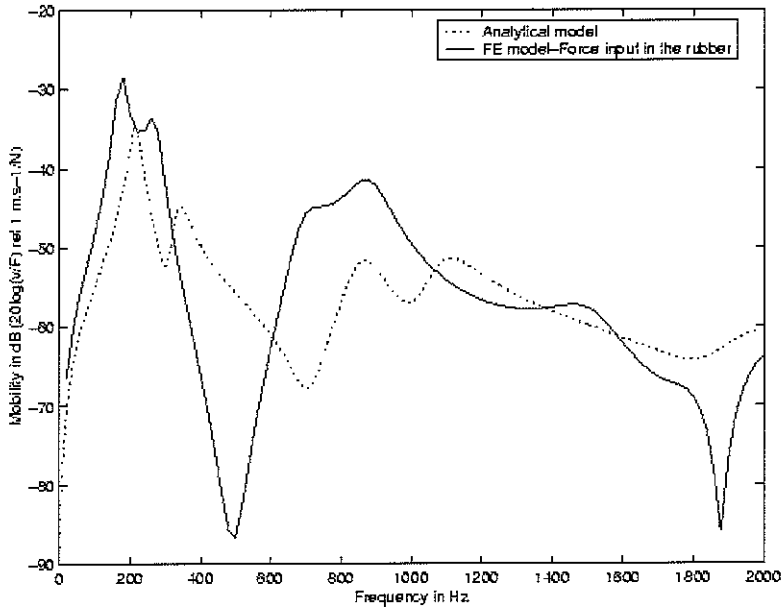

Appendix 25 Transfer mobility between point 2 (input force in the rubber) and point 4 (measured velocity in the aluminium)

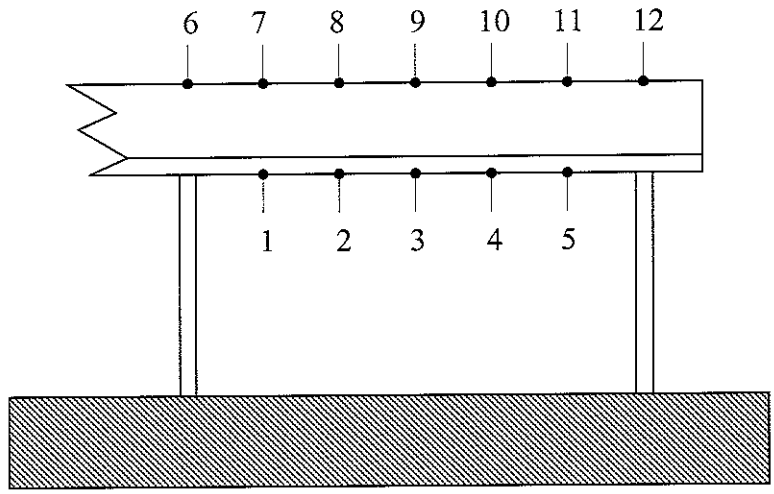

Appendix 26 Position of the different points on the beam for appendices 27 to 50

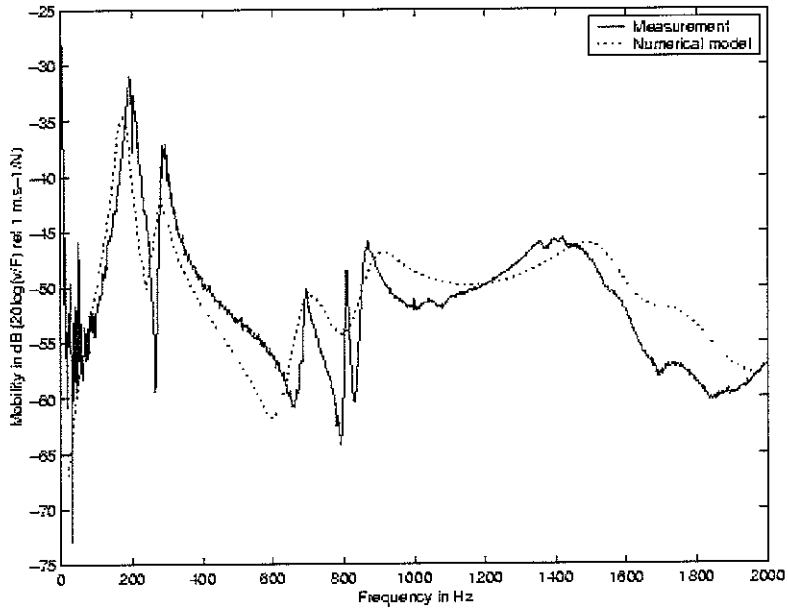

Appendix 27 Mobility between point 3 (input force in the aluminium) and point 1 (measured velocity in the aluminium)

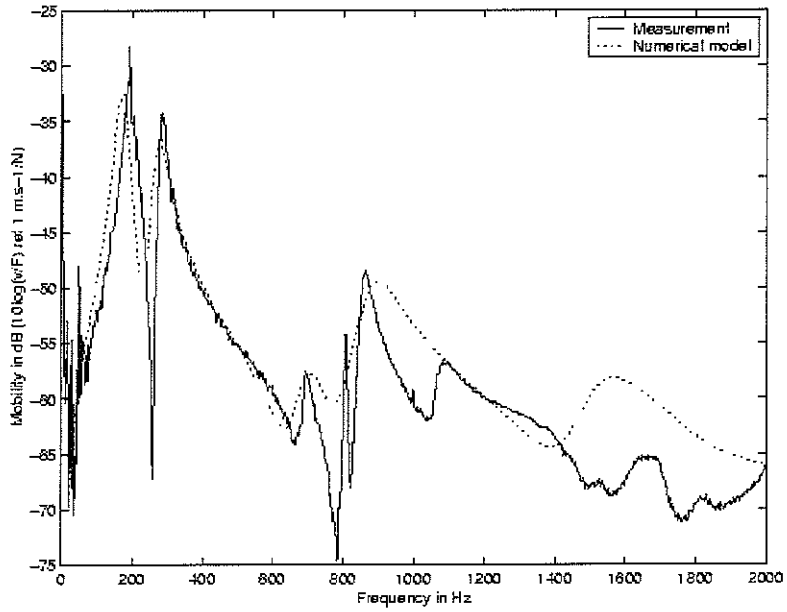

Appendix 28 Mobility between point 3 (input force in the aluminium) and point 2 (measured velocity in the rubber)

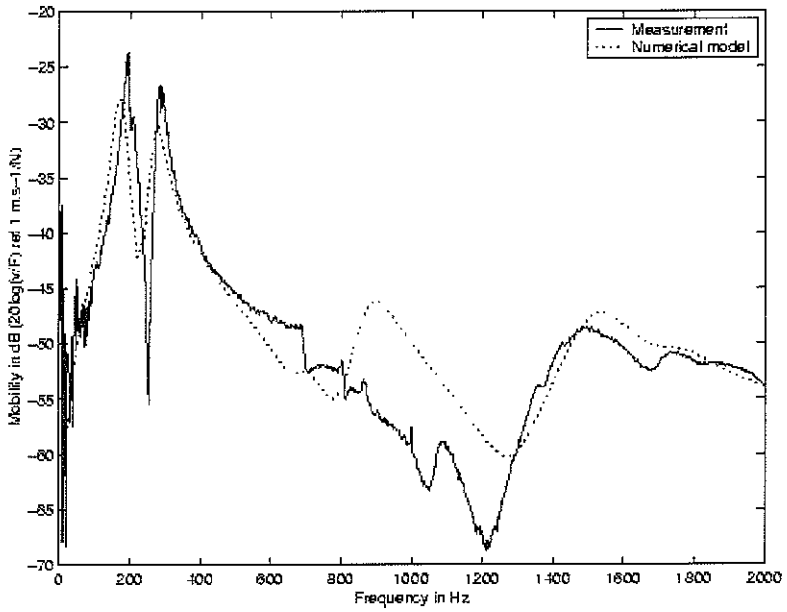

Appendix 29 "Input" mobility at point 3 (point in the aluminium)

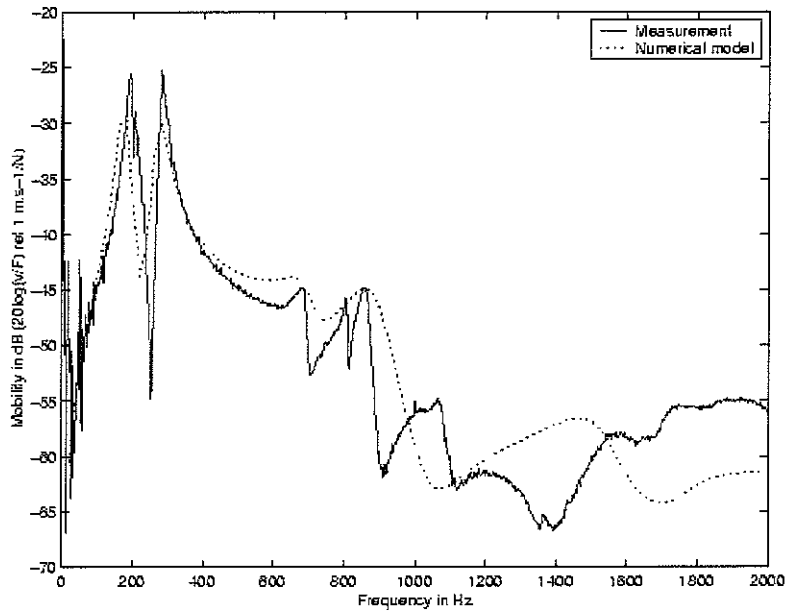

Appendix 30 Mobility between point 4 (input force in the aluminium) and point 3 (measured velocity in the aluminium)

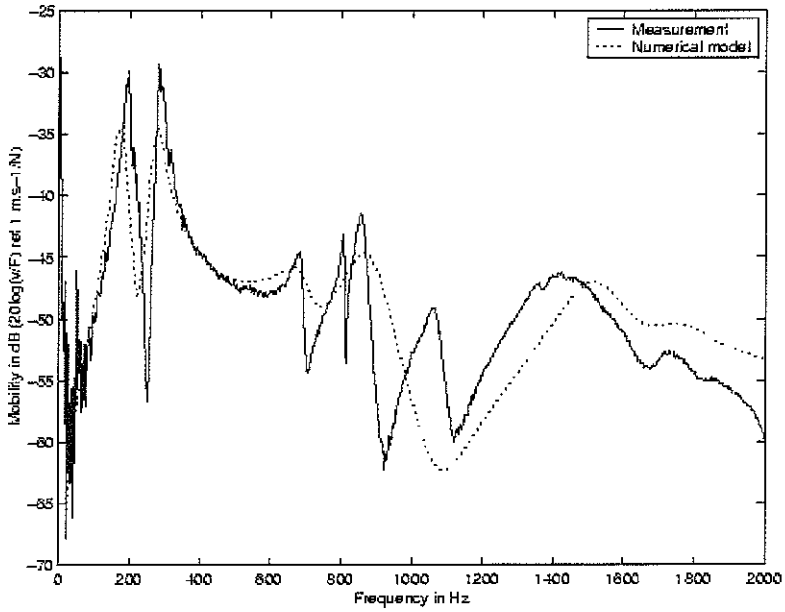

Appendix 31 Mobility between point 3 (input force in the aluminium) and point 5 (measured velocity in the aluminium)

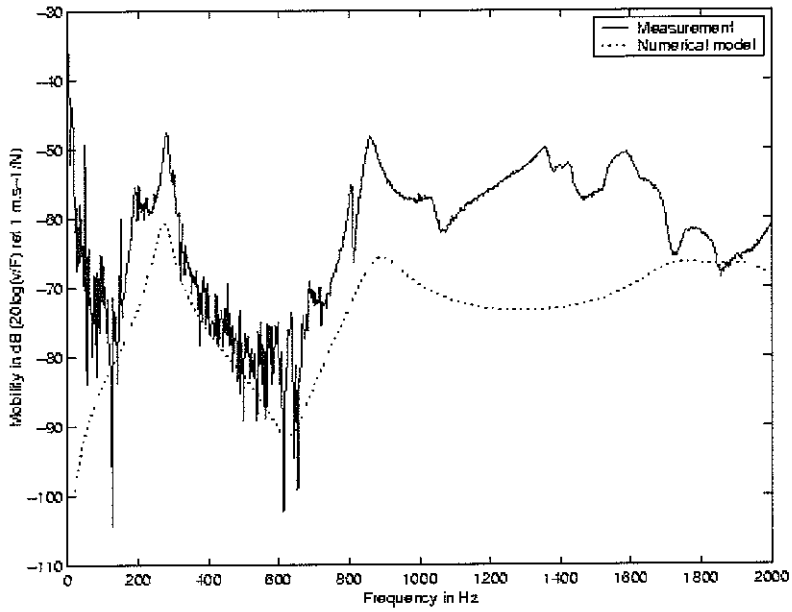

Appendix 32 Mobility between point 3 (input force in the aluminium) and point 6 (measured velocity in the rubber)

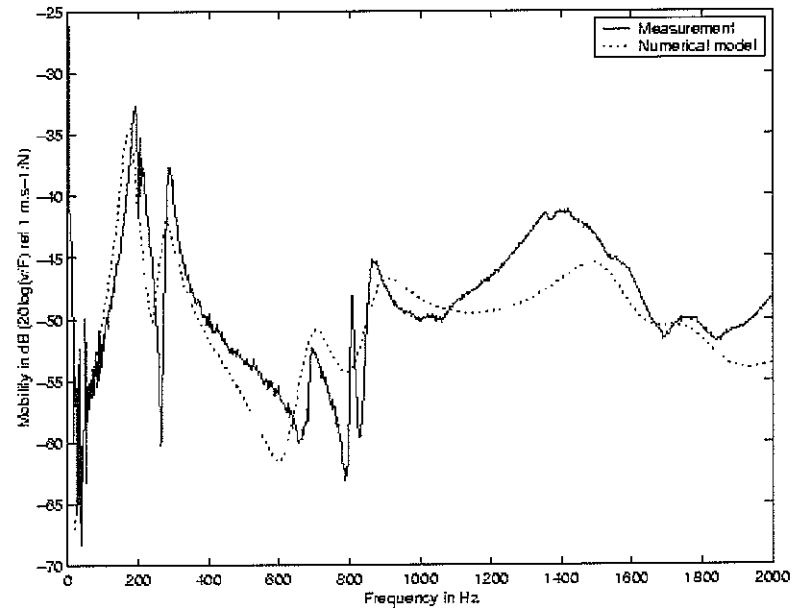

Appendix 33 Mobility between point 3 (input force in the aluminium) and point 7 (measured velocity in the rubber)

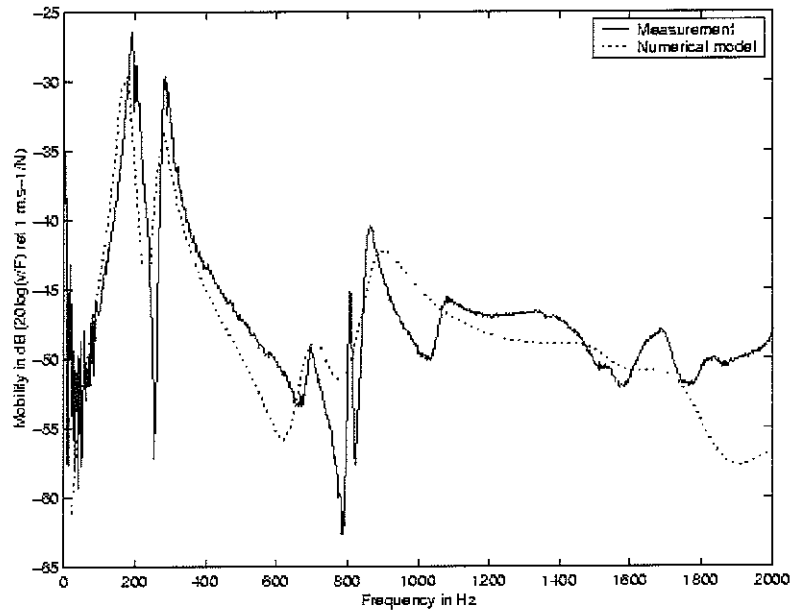

Appendix 34 Mobility between point 3 (input force in the aluminium) and point 8 (measured velocity in the rubber)

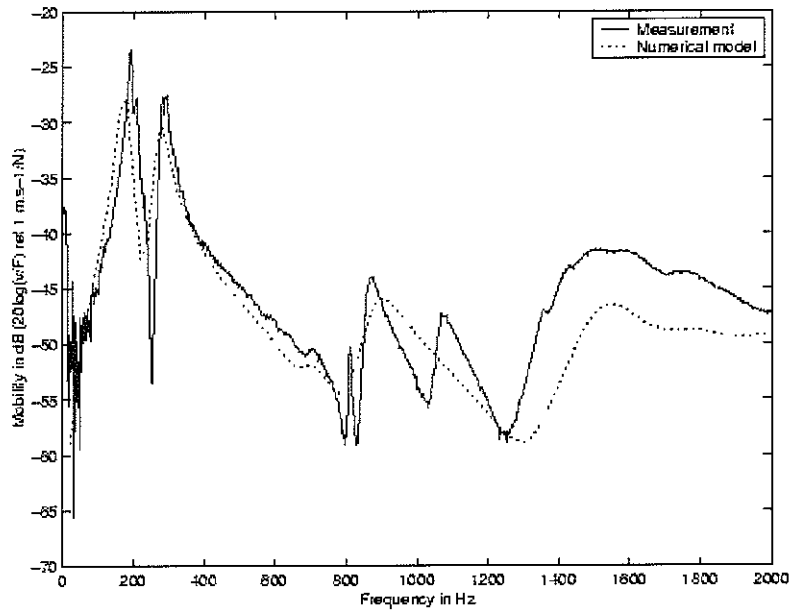

Appendix 35 Mobility between point 3 (input force in the aluminium) and point 9 (measured velocity in the rubber)

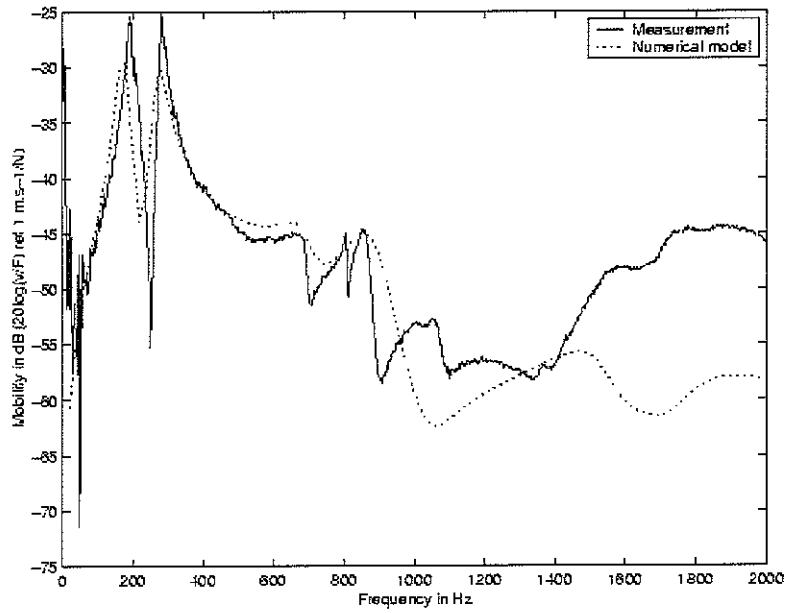

Appendix 36 Mobility between point 3 (input force in the aluminium) and point 10 (measured velocity in the rubber)

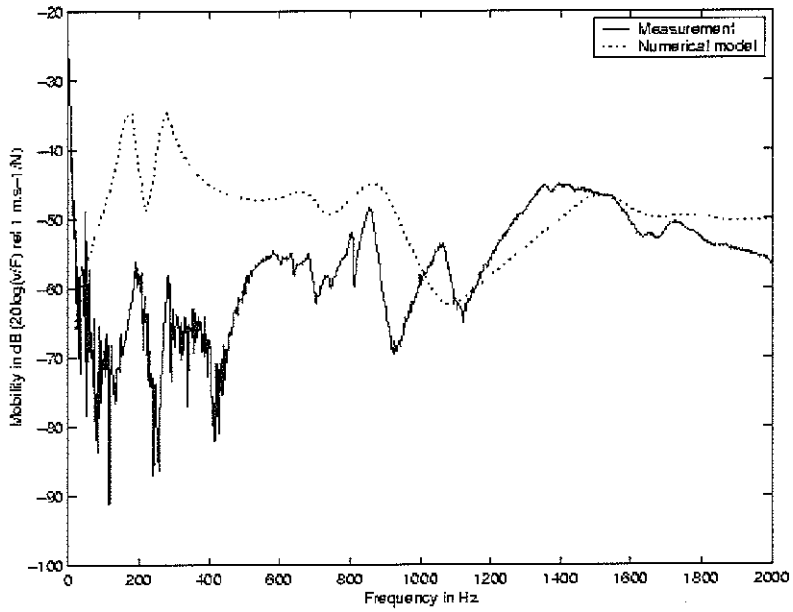

Appendix 37 Mobility between point 3 (input force in the aluminium) and point 11 (measured velocity in the rubber)

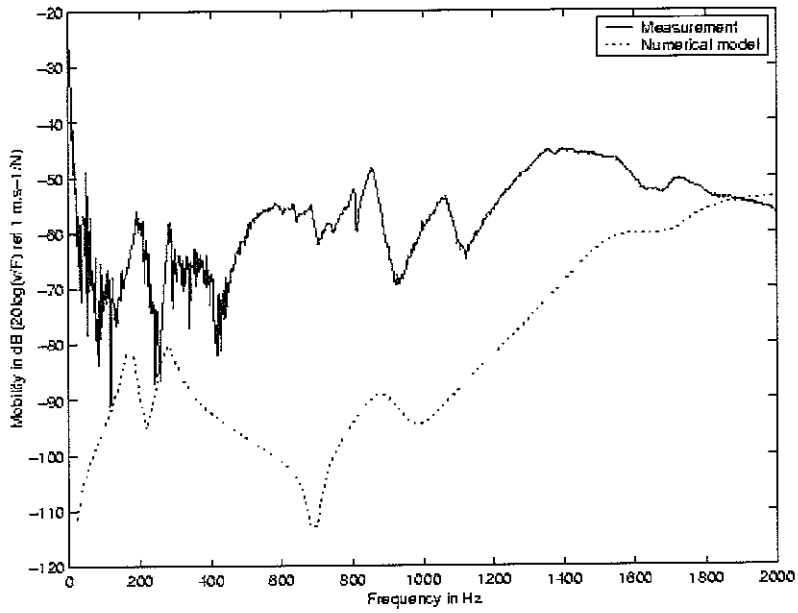

Appendix 38 Mobility between point 3 (input force in the aluminium) and point 12 (measured velocity in the rubber)

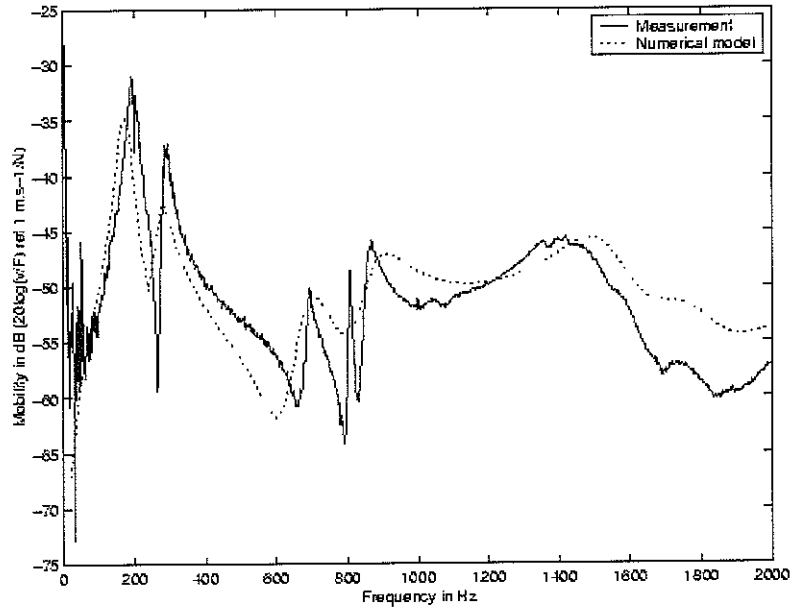

Appendix 39 Mobility between point 9 (input force in the rubber) and point 1 (measured velocity in the aluminium)

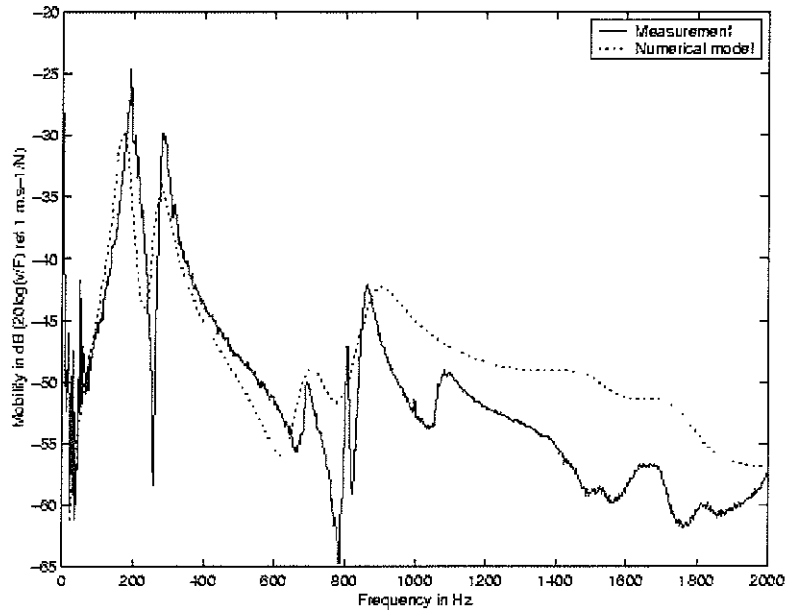

Appendix 40 Mobility between point 9 (input force in the rubber) and point 2 (measured velocity in the aluminium)

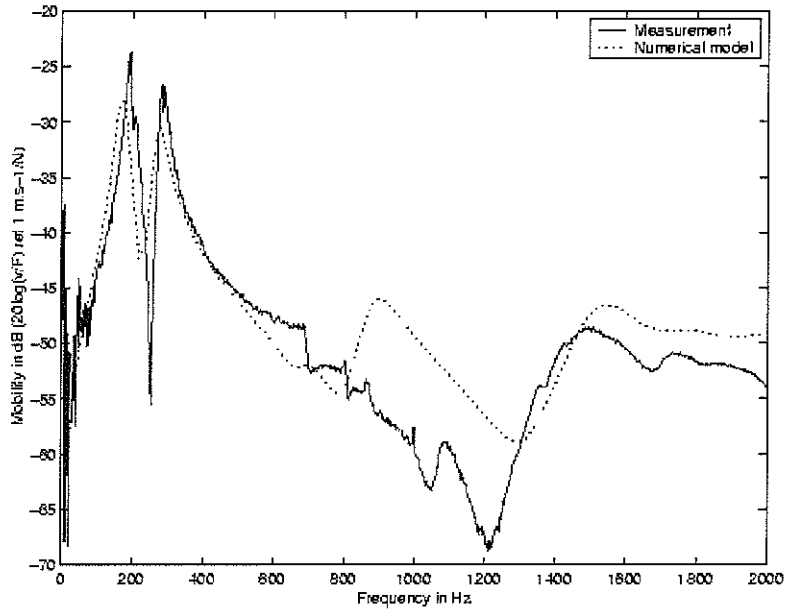

Appendix 41 Mobility between point 9 (input force in the rubber) and point 3 (measured velocity in the aluminium)

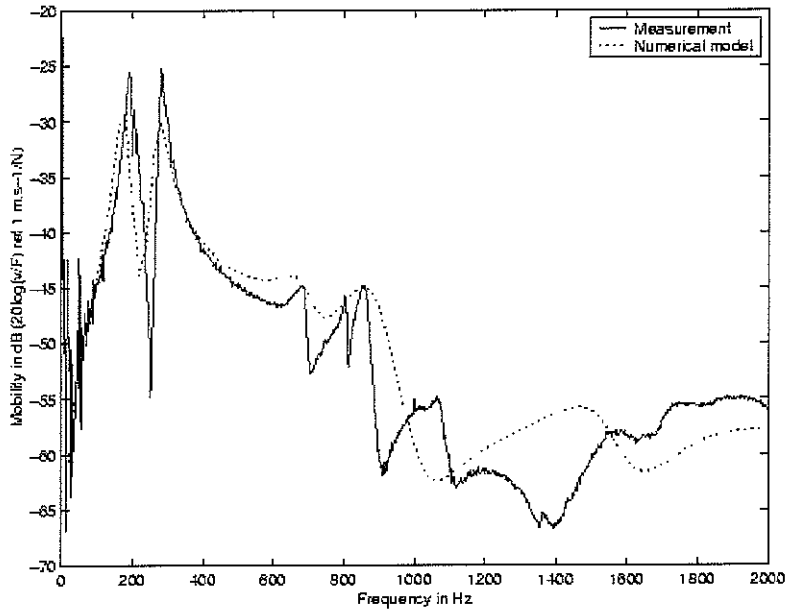

Appendix 42 Mobility between point 9 (input force in the rubber) and point 4 (measured velocity in the aluminium)

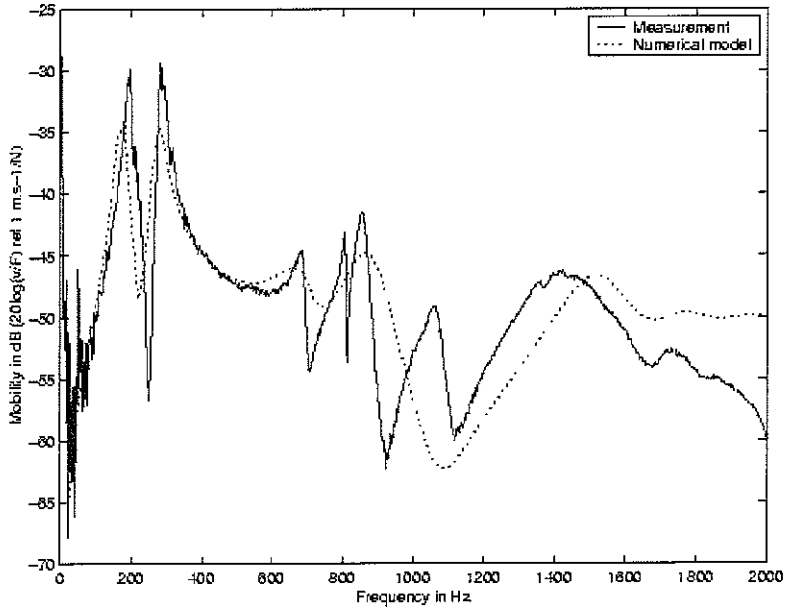

Appendix 43 Mobility between point 9 (input force in the rubber) and point 5 (measured velocity in the aluminium)

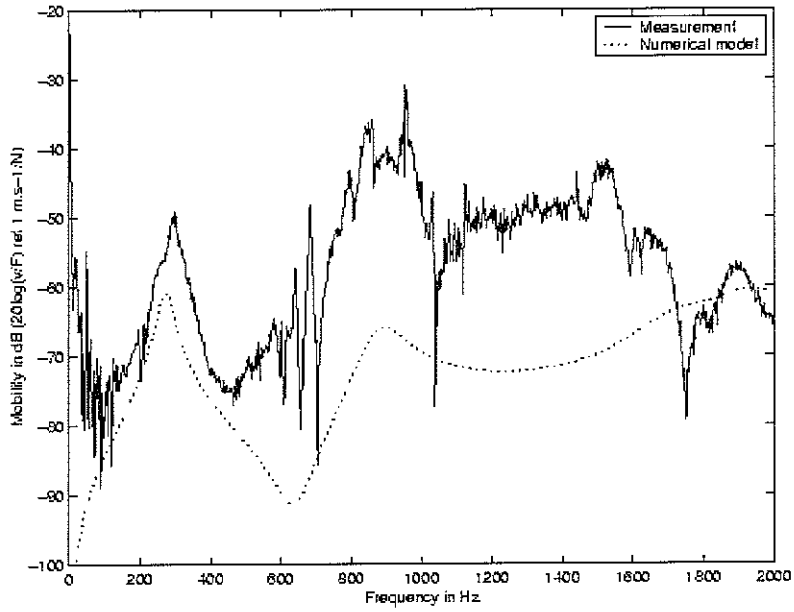

Appendix 44 Mobility between point 9 (input force in the rubber) and point 6 (measured velocity in the rubber

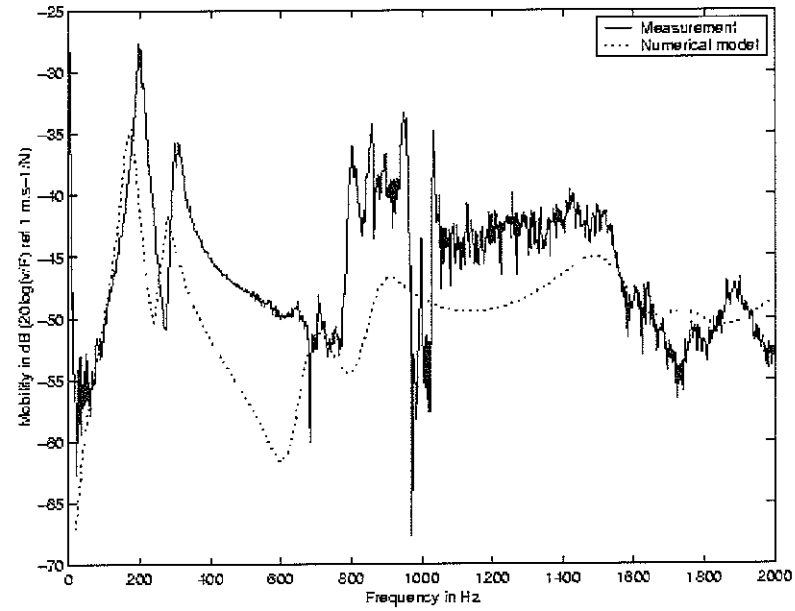

Appendix 45 Mobility between point 9 (input force in the rubber) and point 7 (measured velocity in the rubber)

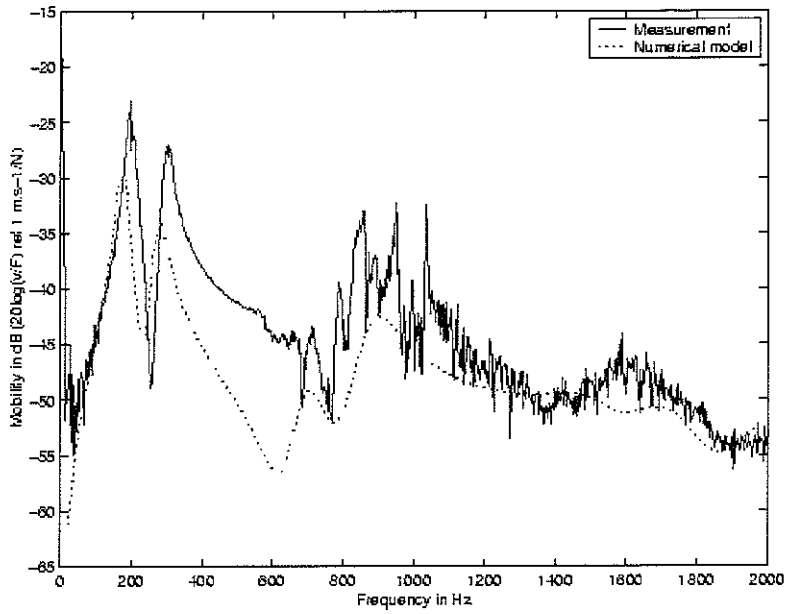

Appendix 46 Mobility between point 9 (input force in the rubber) and point 8 (measured velocity in the rubber)

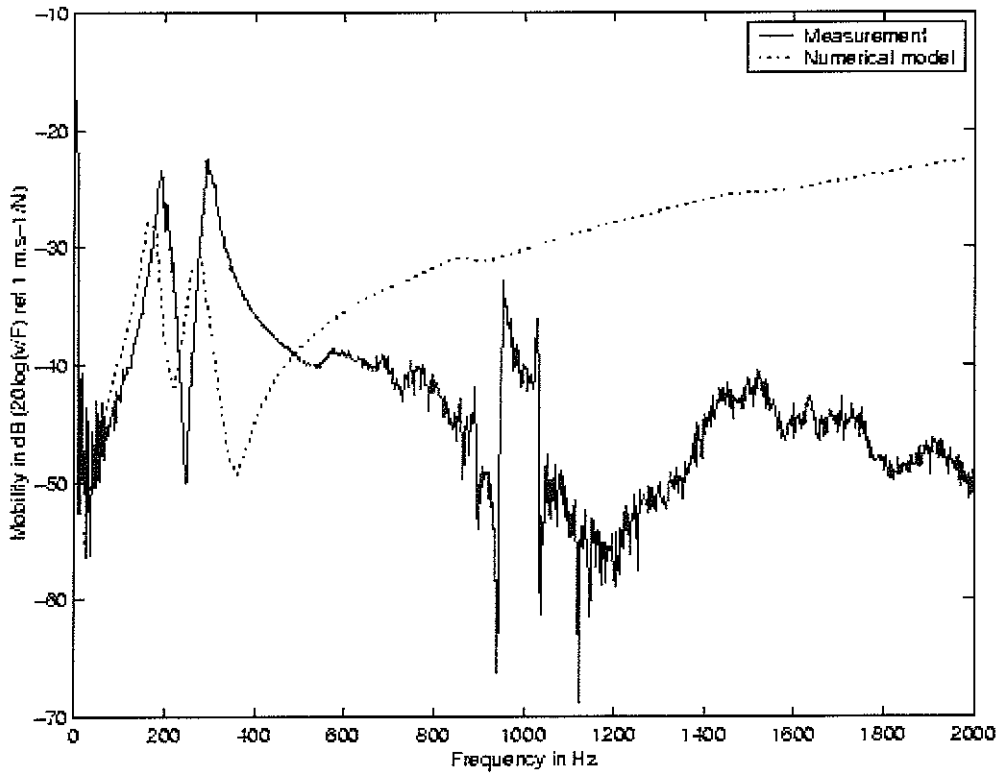

Appendix 47 "Input" mobility at point 9 (point in the rubber)

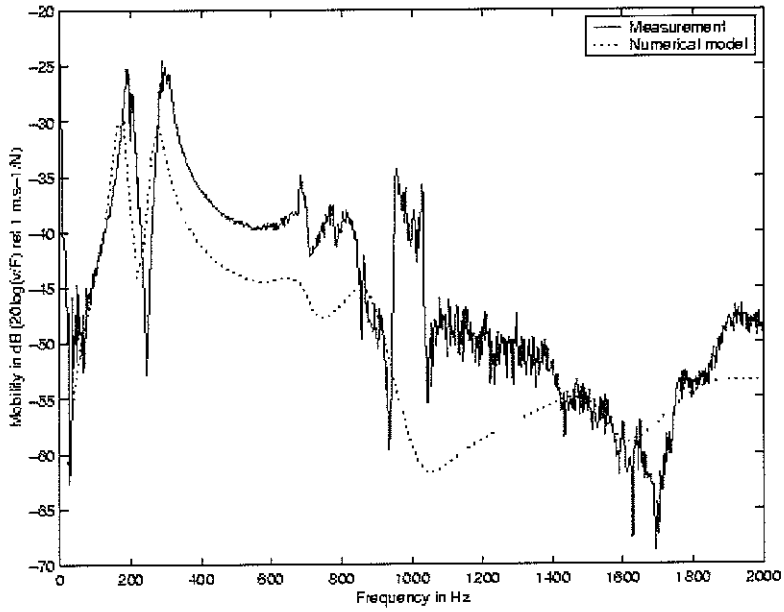

Appendix 48 Mobility between point 9 (input force in the rubber) and point 10 (measured velocity in the rubber)

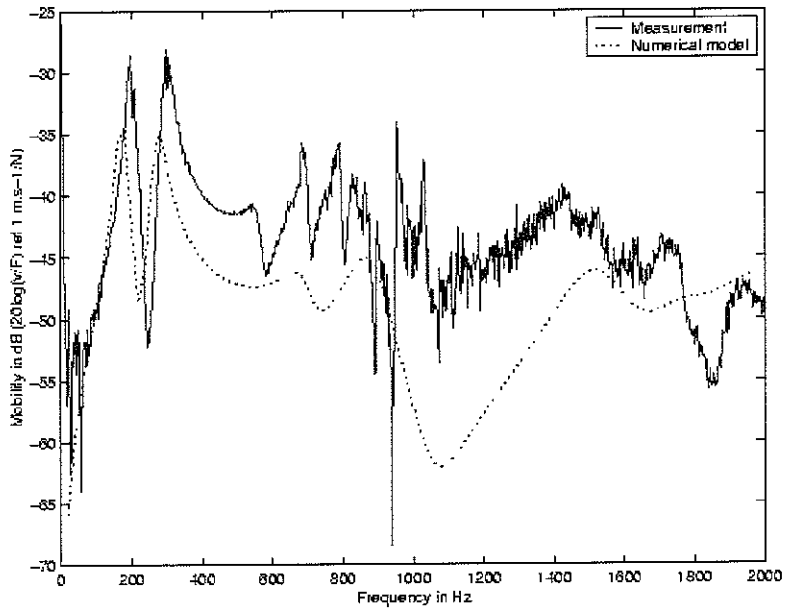

Appendix 49 Mobility between point 9 (input force in the rubber) and point 11 (measured velocity in the rubber)

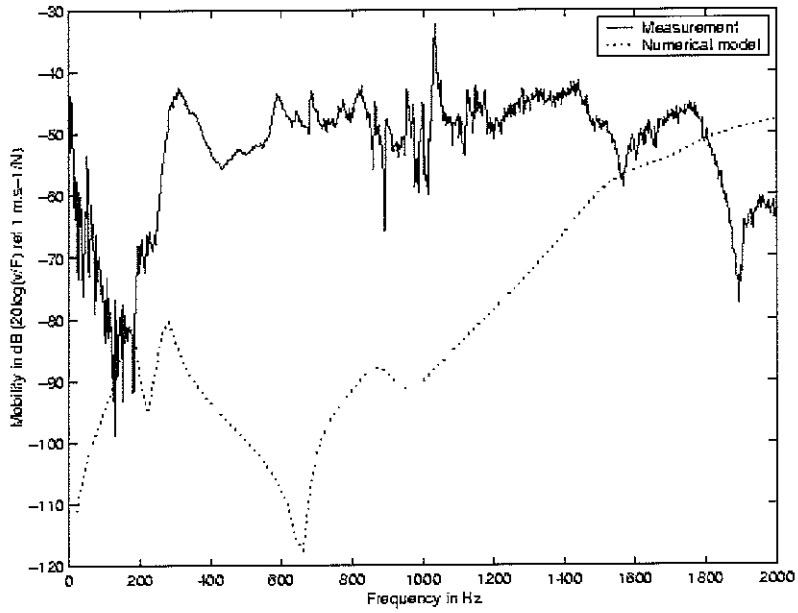

Appendix 50 Mobility between point 9 (input force in the rubber) and point 12 (measured velocity in the rubber)